European Journal of Medicinal Chemistry 48 (2012) 1–15

Contents lists available at SciVerse ScienceDirect

European Journal of Medicinal Chemistry

journal homepage: http://www.elsevier.com/locate/ejmech

Original article

Structure-based design, synthesis and biological evaluation of *N*-pyrazole, *N*′-thiazole urea inhibitors of MAP kinase p38α☆

Matthäus Getlik [a], Christian Grütter [a,b], Jeffrey R. Simard [a], Hoang D. Nguyen [a], Armin Robubi [a], Beate Aust [a], Willem A.L. van Otterlo [c,d,**], Daniel Rauh [a,b,*]

[a] *Chemical Genomics Centre of the Max Planck Society, Otto-Hahn-Strasse 15, D-44227 Dortmund, Germany*
[b] *Fakultät Chemie, Chemische Biologie, Technische Universität Dortmund, Otto-Hahn-Strasse 6, D-44227 Dortmund, Germany*
[c] *Molecular Sciences Institute, School of Chemistry, University of the Witwatersrand, Johannesburg, South Africa*
[d] *Department of Chemistry and Polymer Sciences, Stellenbosch University, Stellenbosch 7600, South Africa*

ARTICLE INFO

Article history:
Received 16 August 2011
Received in revised form
5 November 2011
Accepted 9 November 2011
Available online 18 November 2011

Keywords:
Kinase inhibitors
p38α MAPK
DFG-out

ABSTRACT

In this paper, we present the structure-based design, synthesis and biological activity of *N*-pyrazole, *N*′-thiazole-ureas as potent inhibitors of p38α mitogen-activated protein kinase (p38α MAPK). Guided by complex crystal structures, we employed the initially identified *N*-aryl, *N*′-thiazole urea scaffold and introduced key structural elements that allowed the formation of novel hydrogen bonding interactions within the allosteric site of p38α, resulting in potent type III inhibitors. [4-(3-*tert*-Butyl-5-{[(1,3-thiazol-2-ylamino)carbonyl]amino}-1*H*-pyrazol-1-yl)-phenyl]acetic acid **18c** was found to be the most potent compound within this series and inhibited p38α activity with an IC_{50} of 135 ± 21 nM. Its closest analog, ethyl [4-(3-*tert*-butyl-5-{[(1,3-thiazol-2-ylamino)carbonyl]amino}-1*H*-pyrazol-1-yl)phenyl]acetate **18b**, effectively inhibited p38α mediated phosphorylation of the mitogen activated protein kinase activated protein kinase 2 (MK2) in HeLa cells.

1. Introduction

The p38α mitogen-activated protein kinase (p38α MAPK) is a crucial component for the regulation of many cellular processes, including cell proliferation, differentiation, survival and migration [1]. With the identification of p38α as a key downstream regulator of several inflammatory mediators, the pharmaceutical industry has made tremendous efforts to develop a plethora of p38α inhibitors, but only a few have progressed beyond Phase I clinical trials [2,3]. Recent evidence has shown that p38α may also play a causative role in cancer [1]. Both, the failure of several p38α inhibitors in clinical trials and the indication shift toward cancers highlight the continuous importance of identifying new inhibitors and approaches which target p38α in signaling pathways.

Modern endeavors in kinase drug research focus on the identification and development of inhibitors that target less conserved binding sites or stabilize inactive kinase conformations [4]. One such site is located adjacent to the ATP site and is druggable in several kinases which can adopt the DFG-out conformation [5]. These types of small molecules promise to be advantageous with respect to both selectivity and pharmacological properties in comparison to traditional ATP-competitive inhibitors [5,6].

However, techniques for the identification of such ligands are few in number in kinase inhibitor research, leaving most screening approaches to focus on measuring enzyme activity. Recently, we presented the development of two assay approaches both suitable for the identification of ligands which can stabilize enzymatically inactive kinase conformations [7–10]: a) a displacement assay based on the enzyme fragment complementation (EFC) technology where a peptide fragment of β-galactosidase is fused to a DFG-out binder. This probe binds to the inactive kinase and can be displaced by small molecules targeting the same binding site. The complementation of

Abbreviations: p38α MAPK, p38α mitogen-activated protein kinase; EFC, enzyme fragment complementation; FLiK, fluorescence labels in kinases; Abl, Abelson kinase; MK2, mitogen activated protein kinase activated protein kinase 2.

☆ Atomic coordinates and structure factors for crystal structures of compounds complexed with p38α can be accessed using the following PDB ID codes: Dasatinib **4** (PDB ID: 31FA), **10a** (PDB ID: 31FD), **10c** (PDB ID: 31FE), **10i** (PDB ID: 3PG3), **10e** (PDB ID: 31FC), **18a** (PDB ID: 31FB), and **18c** (PDB ID: 31FF).

* Corresponding author. Fakultät Chemie, Chemische Biologie, Technische Universität Dortmund, Otto-Hahn-Strasse 6, D-44227 Dortmund, Germany. Tel.: +49 0 231 755 7056; fax: +49 0 231 755 7082.

** Corresponding author. Department of Chemistry and Polymer Chemistry, Stellenbosch University, Stellenbosch 7600, South Africa. Tel.: +27 21 808 3344; fax: +27 21 808 3360.

E-mail addresses: wvo@sun.ac.za (W.A.L. van Otterlo), daniel.rauh@tu-dortmund.de (D. Rauh).

0223-5234/$ – see front matter © 2011 Elsevier Masson SAS. All rights reserved.
doi:10.1016/j.ejmech.2011.11.019

the truncated β-galactosidase by the released probe restores its enzymatic activity and allows detection of a chemiluminescent signal [7]. b) The Fluorescence Labels in Kinases (FLiK) technology exploits the flexibility of certain structural elements of kinases – such as the activation loop – which can be labeled with fluorophores that are sensitive to environmental changes. When labeling the activation loop, this advantageous assay system directly reports on conformational changes undergone by the DFG-motif and activation loop, as the kinase switches between its active (DFG-in) and inactive (DFG-out) states. Following the conformation-dependent changes of the emission characteristics of the fluorophore thus allows direct measurement of the dissociation constant (K_D) for ligands [9]. In a high throughput screen of more than 35,000 compounds, we recently applied the FLiK approach to p38α and identified several new scaffolds as potent binders which inhibit p38α activity. Complex crystal structures revealed that the class of *N*-aryl, *N*′-thiazole-ureas binds, albeit weakly, within the allosteric pocket of p38α (K_Ds = 13–48 μM), stabilizes the DFG-out conformation and inhibits p38α activity (IC_{50}s = 12–75 μM) [11]. These *N*-aryl, *N*′-thiazole-urea hits all share a conserved benzyloxy-ethyl substituent at position 4 of the thiazole which seems to be crucial for binding (Fig. 1). Additionally, the urea moiety forms the expected interactions with the backbone of Asp168 and the side chain of Glu71. However, the bent conformation of the benzyloxy-ethyl moiety within the hydrophobic subpocket behind the gatekeeper residue clearly forces the urea pharmacophore into a tilted geometry when compared to the binding mode of BIRB-796 and may prevent this compound class from binding more tightly to the kinase [11].

We decided to pursue further optimization attempts of this scaffold, since we expected to be able to significantly increase the binding affinity of these thiazole-ureas by introducing additional functional groups and/or extending them to type II inhibitors. Moreover, these compounds have never been identified before as stabilizers of the inactive conformation of p38α (or other kinases) and they therefore represent a novel compound class for this type of binding mode. Together, these initial findings stimulated the further investigation of the thiazole-urea scaffold and led to the development of novel type III inhibitors of p38α kinase. Herein, we report the systematic structure-based design, synthesis and structure–activity relationships (SAR) of *N*-pyrazole, *N*′-thiazole-ureas as potent type III inhibitors of p38α kinase. We demonstrate through biochemical and structural analysis that chemical modifications of the thiazole-urea scaffold allow us to exploit its structural flexibility and to specifically address the hinge region and the allosteric site, respectively. Furthermore, we demonstrate that one compound of the series, **18b**, potently inhibits the enzymatic activity of p38α in HeLa cells by blocking downstream phosphorylation of MK2.

2. Chemistry

We synthesized a focused collection of p38α inhibitors based on the *N*′-thiazole-urea scaffold using a convergent synthesis route which allowed the facile combination of previously prepared synthons. Detailed synthetic procedures for all compounds are described in the Experimental Section. Briefly, synthesis of the carbamate **6** was achieved by Boc-protection of ethyl (2-amino-1,3-thiazol-4-yl)acetate. The reduction of **6** with excess $NaBH_4$ at 0 °C led to the alcohol **7**. Treatment of this compound with NaH in THF and subsequent addition of the respective benzyl bromides at room temperature, followed by Boc-deprotection with 4 M HCl in dioxane, completed the formation of 4-substituted 2-amino-thiazoles **8a**–**c** (Scheme 1). In contrast, the reaction of **7** with 3-(bromomethyl) pyridine mainly yielded the undesired *N*-alkylated product. Alternatively, the alcohol **7** was converted into the corresponding tosylate which was then displaced by the anion generated from 3-pyridinemethanol to give *tert*-butyl 4-[2-(3-pyridinylmethoxy) ethyl]-1,3-thiazol-2-ylcarbamate **10** in moderate yield over two steps (Scheme 1).

Synthesis of nitriles **12a**,**b** was achieved by reaction of methyl cyclopropanecarboxylate or methyl cyclopentanecarboxylate with acetonitrile, after addition of NaH [12]. Hydrazines **14a**,**b** were obtained through nitrosation of aminophenyl acetic acids **13a**,**b**, followed by reduction with $SnCl_2$ (Scheme 2) [12]. Pinner-type condensation of the nitriles **12a**–**c** and the hydrazine hydrochlorides **14a**,**b**, in the presence of catalytic amounts of hydrochloric acid in ethanol, then led to the formation of 5-amino-pyrazoles as described in the patent literature [12]. The trichloroethyl carbamates **15a**–**f** were subsequently prepared by using a procedure described before [13] in which urea formation was completed by the reaction of **15a**–**f** with 2-amino-thiazoles **8a**–**c** in the presence of DIPEA in DMSO at 60 °C to afford the compounds **16a**–**h** (Scheme 3). Finally, compounds **16d**–**h** were obtained by the conversion of the ethyl esters into the corresponding carboxylic acids using LiOH in methanol/water (Scheme 3). *N*-[3-*tert*-Butyl-1-(4-methylphenyl)-1*H*-pyrazol-5-yl]-*N*′-{4-[2-(3-pyridinylmethoxy)ethyl]-1,3-thiazol-2-yl}urea **16i** was synthesized starting from *tert*-butyl 4-[2-(3-pyridinylmethoxy)ethyl]-1,3-thiazol-2-ylcarbamate **10** which was

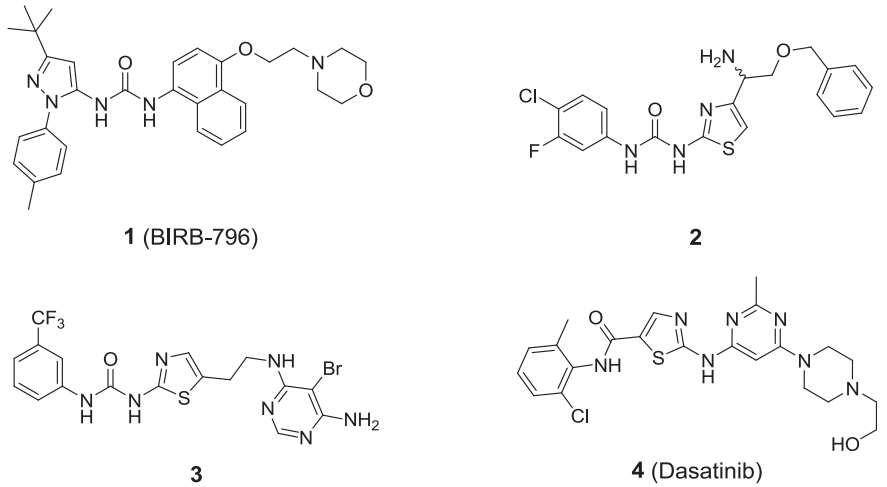

Fig. 1. Chemical structures of the potent p38α inhibitor BIRB-796 **1**, the representative **2** of the initially identified *N*-aryl, *N*′-thiazole-ureas, the structurally related Aurora kinase A inhibitor **3**, and the dual-specific Abl/Src inhibitor dasatinib **4**, that also binds to p38α.

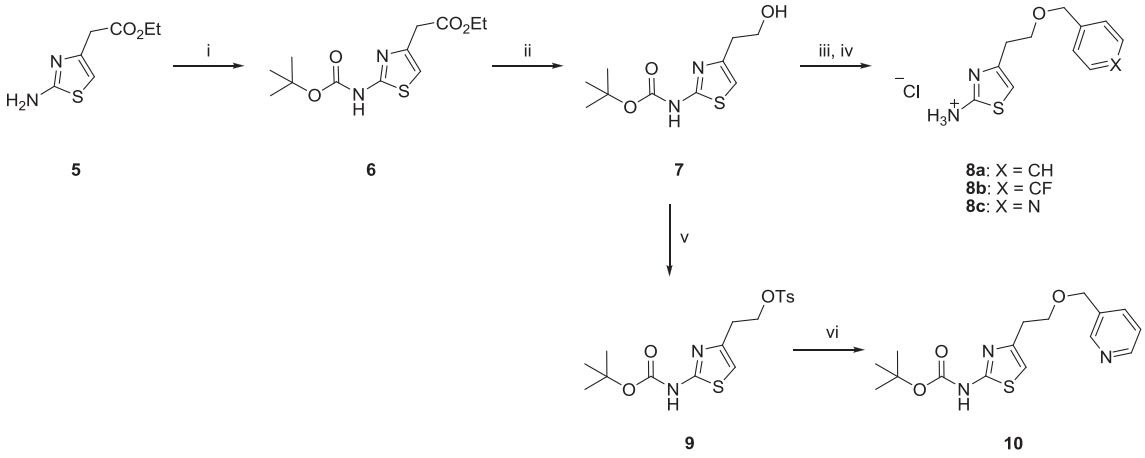

Scheme 1. Reagents and conditions: (i) Boc_2O, NEt_3, THF, cat. DMAP, 0 °C; (ii) $NaBH_4$, EtOH, 0 °C; (iii) NaH, benzyl bromides, THF, rt; (iv) HCl (4 M) in dioxane, rt; (v) TsCl, pyridine, rt; (vi) NaH, 3-pyridinemethanol, THF, rt.

first treated with 4 M HCl in dioxane to remove the *tert*-butyloxycarbonyl group. The resulting amine was then coupled with carbamate **15a** (Scheme 4). In addition, compounds **18a**,**b** were obtained under similar conditions through the reaction of 2-aminothiazole **17** with **15a** or **c**, respectively. **18b** was then treated with LiOH in a methanol/water mixture to give the carboxylic acid **18c** (Scheme 5). The addition of **8a** to isocyanate **19** under basic conditions yielded *N*-{4-[2-(benzyloxy)ethyl]-1,3-thiazol-2-yl}-*N*′-[4-chloro-3-(trifluoromethyl)phenyl]urea **20** (Scheme 6). Finally, 3-fluoro-5-morpholinobenzoic acid **21** and 2-aminothiazole **8a** were coupled under standard peptide coupling conditions using HBTU to give N-{4-[2-(benzyloxy)-ethyl]-1,3-thiazol-2-yl}-3-fluoro-5-(4-morpholinyl)benzamide 22 in acceptable yield (Scheme 7).

3. Pharmacology

3.1. Biochemical validation

To confirm and validate our synthesized inhibitors, we first measured their K_D-values using the p38α-FLiK assay (Table 1) [9]. The binding data confirmed the expected affinities and supported the inhibitor development. Utilizing structure-based design principles we were able to increase the binding affinities of the initial hit compounds by 70-fold. Furthermore, we employed the p38α FLiK system to investigate the binding kinetics of **18c**, the most potent compound within the series (Fig. 5). As reported, BIRB-796 and pyrazolo-urea based p38α inhibitors belong to the slowest dissociating inhibitors of p38α [14]. Binding of these ligands induces conformational changes of the kinase (DFG-in/DFG-out) which results in the slow binding behavior of this compound class. We confirmed slow binding also for our novel thiazole-urea based inhibitor **18c** and found the dissociation constant k_{off} to be 1.56×10^{-3} s^{-1}, a value which compares well to the previously determined dissociation constants for pyrazolo-urea based type III inhibitors of p38α [9]. As binding affinities of BIRB-796 and related type III inhibitors are predominantly governed by their slow dissociation rates [14], this binding behavior might also be responsible for the high affinity of **18c**. Additionally, we performed enzyme activity assays for p38α with the most promising compounds to confirm inhibition of enzymatic phosphotransfer and to support the previously obtained binding data (Table 2). We found both IC_{50}s and K_Ds to follow the same trends, although the absolute values were not identical. Within the compound collection **18c** displayed the highest affinity, which was also confirmed by the lowest IC_{50}-value measured.

3.2. Cellular evaluation

To assess p38α inhibition in a cellular system, we monitored the ability of **18c** to inhibit the phosphorylation of mitogen activated

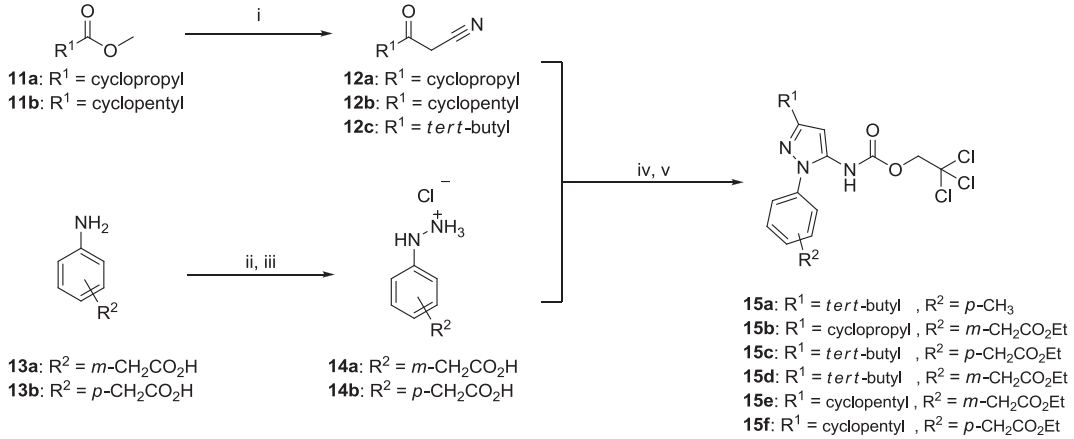

Scheme 2. Reagents and conditions: (i) NaH, MeCN, THF, 70 °C; (ii) HCl, $NaNO_2$, H_2O, 0 °C; (iii) $SnCl_2$, conc. HCl, rt; (iv) conc. HCl (cat.), EtOH, reflux; (v) TrocCl, H_2O, EtOAc, NaOH, 0 °C to rt.

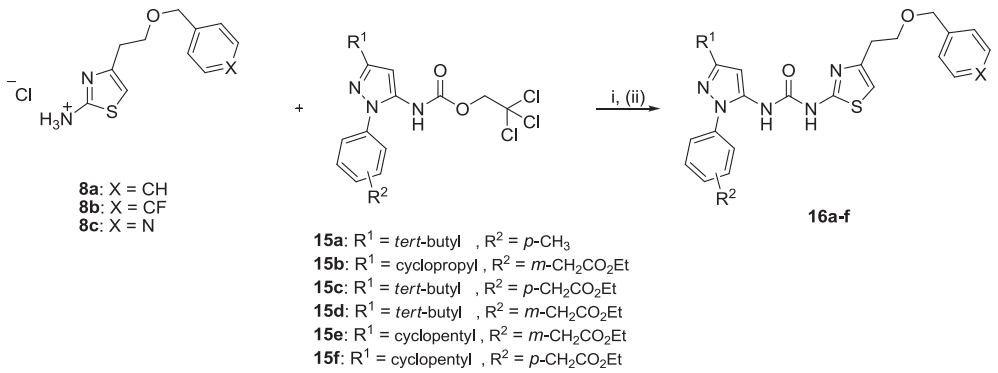

Scheme 3. Reagents and conditions: (i) DIPEA, DMSO, 60 °C; only for derivatives **16d**–**f**: (ii) LiOH, MeOH/H_2O (1:1), rt (see Table 1).

protein kinase activated protein kinase 2 (MK2), a well known substrate of p38α (Fig. 6) [15]. MK2 and p38α form a stable heterodimer in the nucleus of a cell. Upon stress signaling, phosphorylation of p38α leads to disruption of this protein complex. However, activated p38α can again bind to and phosphorylate MK2 at its phosphorylation sites and induces a subsequent conformational change of MK2 resulting in the exposition of its nuclear export signal. This initiates the export of the p38α-MK2-complex into the cytoplasm where further substrates, such as transcription factors and heat shock proteins, are phosphorylated. Thus, MK2 determines cellular localization of p38α and at the same time serves as an effector of p38α by phosphorylating further substrates [16,17]. Thus, HeLa cells were treated for 2 h with different concentrations of inhibitor, or vehicle (DMSO) and then stimulated with anisomycin (10 mg/mL) for 30 min. We monitored the phosphorylation state of Thr334 (a phosphorylation site in the C-terminal domain of MK2 which controls binding of protein substrates and nuclear localization) [18,19].

Despite strong *in vitro* inhibition of p38α activity (135 ± 21 nM) by **18c** (Table 2), we observed no *in vivo* effect on the phosphorylation of MK2 and attributed this lack of efficacy to the poor cell permeability of **18c** due to its highly charged carboxylic acid function. To improve the cell permeability we therefore utilized the ethyl ester derivative **18b**. To our satisfaction, in spite of a 5-fold lower *in vitro* activity when compared to **18c** (Table 2), **18b** effectively inhibited MK2 phosphorylation in a concentration-dependent manner with a cellular IC_{50} of 6 μM (Fig. 6).

4. Results

4.1. Structure-guided design of potent type II and type III inhibitors for p38α

We recently employed our newly developed p38α-FLiK assay system to perform a HTS of more than 35,000 compounds [11]. In this screening campaign we were able to identify several hits amongst which we found the class of *N*-aryl, *N*′-thiazole-ureas (Fig. 1) [11]. Structurally related compounds have been reported to inhibit Aurora kinase activity, with the difference being that these compounds bind in the ATP site of the kinase in an active conformation (Fig. 2). Interestingly, the marketed thiazole-based Abl/Src inhibitor dasatinib has also been shown to bind to p38α [20]. We used protein X-ray crystallography to solve the structure of dasatinib in complex with p38α (Fig. 2), and confirmed an ATP-competitive binding mode which is also observed in both cSrc (PDB ID: 3G5D) [13] and Abl (PDB ID: 2GQG) [21]. Binding of dasatinib to p38α is identical to the reported structures for cSrc and Abl, despite the fact that the hinge region of p38α is one amino-acid shorter. The inhibitor contacts the hinge-region by forming three hydrogen bonds: one between the nitrogen of the aniline moiety and the gatekeeper side chain (Thr106), the second between the nitrogen atom of the thiazole core and the backbone nitrogen of Met109, and the third one between the secondary amine which bridges the thiazole- and pyrimidine ring and the backbone carbonyl of Met109. Moreover, the inhibitor forms a water-mediated hydrogen bond to Lys53 of the glycine-rich loop. The solubilizing ethoxypiperazine moiety of the inhibitor is solvent exposed and points out of the ATP binding-site. Although dasatinib is a classical type I binder, the conformation of the DFG-motif and the activation loop of p38α is rather flexible, resulting in a fuzzy electron density for this structural element. Therefore, the activation loop could not be modeled, unlike for cSrc [13] and Abl [21] that exhibit a clear DFG-in conformation when dasatinib is bound.

These findings further highlight the unique type III binding mode of the thiazole-urea scaffold in p38α which was not observed before for this compound class and together with the moderate binding affinities of the initial hit compounds stimulated further inhibitor development. We believed the thiazole-urea scaffold to be a valuable starting point, as substituted thiazoles can be found in many natural products, pharmaceuticals and agrochemical agents and might represent a biologically privileged chemical entity [22].

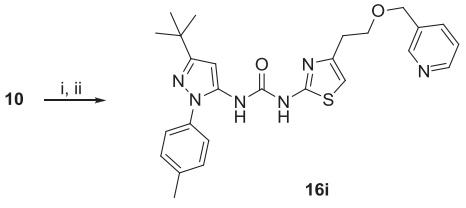

Scheme 4. Reagents and conditions: (i) HCl (4 M) in dioxane, rt; (ii) **15a**, DIPEA, DMSO, 60 °C.

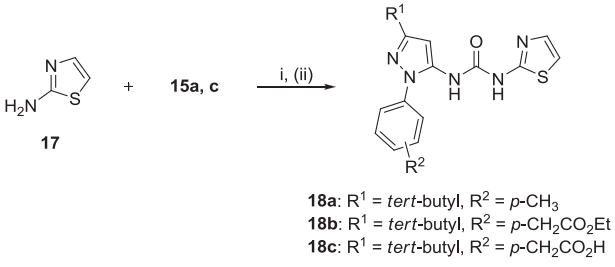

Scheme 5. Reagents and conditions: (i) DIPEA, DMSO, 60 °C; (ii) to obtain **18c**: **18b**, LiOH, H_2O/MeOH, (1:1), rt.

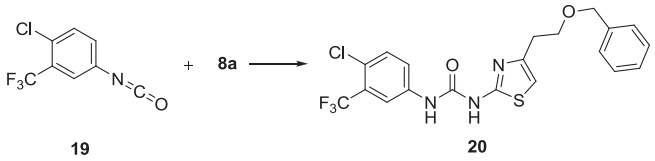

19 20

Scheme 6. Reagents and conditions: DIPEA, DCM, rt.

Guided by the structure of the original hit **2** in complex with p38α (Fig. 2) we retained the central thiazole-urea pharmacophore and modified the substituents on both the thiazole ring and the *N*-urea nitrogen atom to investigate structure–activity relationships (SAR). Since the 4-benzyloxy-ethyl moiety appears to significantly contribute to the affinity of **2** and other identified hits, we only removed the amine-substituted chiral center which did not appear to form critical hydrogen bonding interactions. Next, we decorated the *N*-urea nitrogen atom with various hydrophobic substructures commonly employed in kinase inhibitor research which project into the allosteric site (Table 1) [5]. The introduction of the 3-*tert*-butyl-1-*p*-tolyl-1*H*-pyrazole moiety generated **16a**, which displayed a 40-fold increase in affinity when compared to the parent compound (Table 1). Modeling studies (data not shown) encouraged us to investigate the use of cycloalkane substituents at position 3 of the pyrazole to more efficiently occupy the hydrophobic part of the allosteric pocket. Subsequent attempts to introduce cyclopropyl (in **16d**) or cyclopentyl moieties (in **16g** and **h**) unfortunately did not result in better binding affinities.

To learn more about the critical binding interactions of this compound class, we determined the crystal structure of **16a** in complex with p38α. This structural study confirmed the main binding interactions previously observed for **2**. Moreover, it helped to understand the conformation of the inhibitor when bound to p38α (Fig. 3). The urea moiety forms the typical hydrogen bonding interactions with Asp168 of the DFG-motive and the side chain of Glu71 (located within helix C), interactions typically observed for various type II/III urea-based inhibitors [7,9,13,14]. An additional hydrogen bond is formed between the nitrogen atom of the thiazole ring and the catalytic Lys53. This interaction might stabilize the folded conformation of the 4-benzyloxy-ethyl moiety of the inhibitor within the hydrophobic back pocket behind the gatekeeper residue. Interestingly, this hydrogen bond together with the hydrophobic interactions formed by the 4-benzyloxy-ethyl moiety lead to the reorientation of the entire thiazole-urea pharmacophore when compared to known type III urea-based p38α-inhibitors [14] and might prevent the inhibitor from adopting an orientation appropriate for the formation of ideal hydrogen bonds with Asp168 and Glu71.

Although the 4-benzyloxy-ethyl substituent appears to contribute to the affinity and thus to be crucial for binding of the previously identified thiazole-urea hits, the bent conformation of this group within the subpocket clearly forces the urea moiety into a tilted geometry when aligned with the more optimal binding mode of BIRB-796 [11]. To relieve this strain, we set out to develop

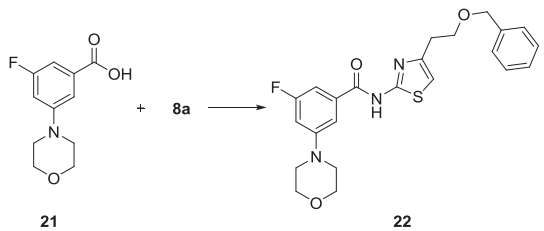

21 22

Scheme 7. Reagents and conditions: HBTU, DIPEA, DMF, rt.

Table 1
Focused library of *N*-pyrazole, *N*′-thiazole urea inhibitors and binding affinities (K_D) for p38α.[a]

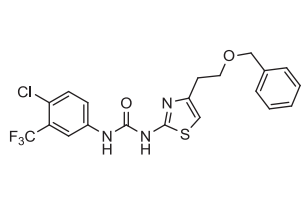

20

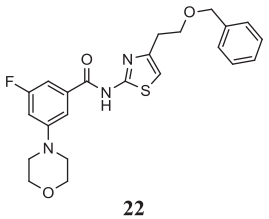

22

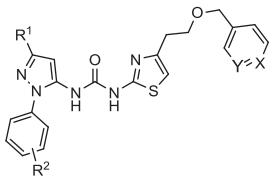

16a-i

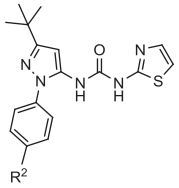

18a-c

Compound	R^1	R^2	X	Y	K_D [nM]
1	–	–	–	–	7.5[9] ± 2.3
2	–	–	–	–	13400 ± 2300
20	–	–	–	–	Poor solubility
22	–	–	–	–	No binding
18a	–	Me	–	–	990 ± 110
18c	–	*p*-CH_2CO_2H	–	–	196 ± 38
18b	–	*p*-CH_2CO_2Et	–	–	675 ± 58
16a	*tert*-butyl	*p*-CH_3	CH	CH	382 ± 65
16b	*tert*-butyl	*p*-CH_3	CF	CH	303 ± 60
16c	*tert*-butyl	*p*-CH_3	N	CH	586 ± 98
16i	*tert*-butyl	*p*-CH_3	CH	N	1656 ± 107
16d	cyclopropyl	*m*-CH_2CO_2H	CH	CH	14700 ± 5700
16e	*tert*-butyl	*p*-CH_2CO_2H	CH	CH	287 ± 42
16f	*tert*-butyl	*m*-CH_2CO_2H	CH	CH	920 ± 11
16g	cyclopentyl	*m*-CH_2CO_2H	CH	CH	580 ± 139
16h	cyclopentyl	*p*-CH_2CO_2H	CH	CH	901 ± 61

[a] K_D-values were measured using the p38α FLiK assay. The activation loop of p38α was labeled with acrylodan as previously described [9]. The fluorescent labeled protein was incubated with inhibitor for 5 h before fluorescence intensities were measured at two wavelengths, 514 nm and 468 nm respectively. The ratio of both values was plotted against inhibitor concentration and the K_D-values were obtained from the resulting binding curves.

type II inhibitors which address the hinge region via their 4-benzyloxy-ethyl substituent. We thus replaced the hydrophobic phenyl ring with a more polar pyridine moiety (as in **16c** and **i**) and observed the expected flip of this linker entity into the ATP binding site (Fig. 3). Compared to the previously crystallized ligands, the central thiazole core of inhibitors **16c** and **i** shifts about 2 Å away from the DFG-motif. This results in the relief of the geometrical strain and allows the urea pharmacophore to adopt a more favored orientation. However, this reorientation also leads to the disruption of the hydrogen bond between the thiazole-nitrogen and Lys53.

Table 2
IC_{50}-values for inhibited enzyme activity of p38α.[a]

Compound	IC_{50} [nM]
18c	135 ± 21
18b	639 ± 67
16i	3641 ± 486
1	8 ± 2

[a] IC_{50}-values were measured with the HTRF® KinEASE assay from Cisbio according to the manufacturer's instructions. Enzymatically active p38α was incubated with compound for 2 h and phosphorylation of ATF-2 peptide was followed.

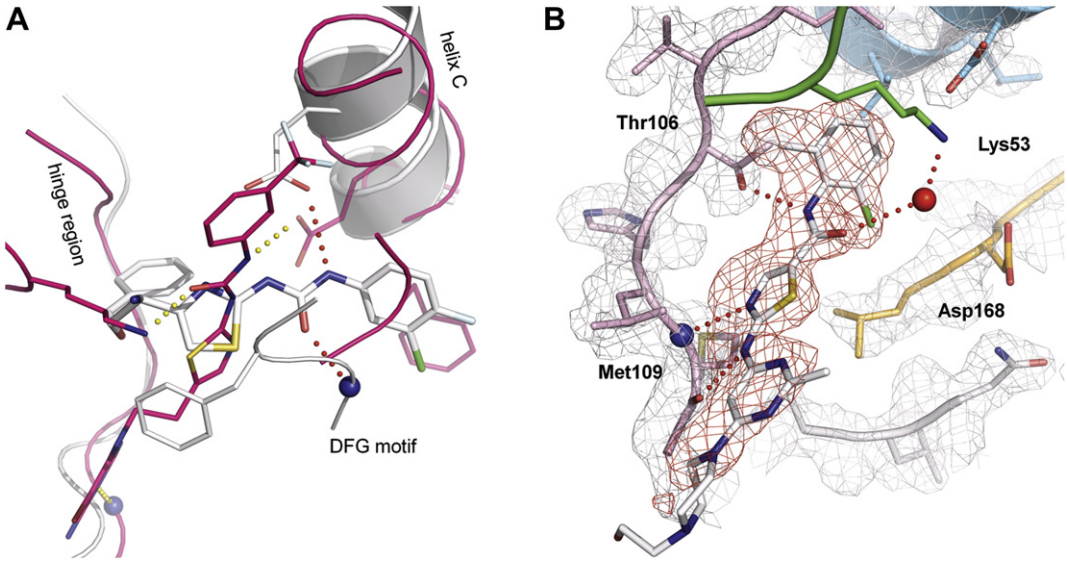

Fig. 2. (A) Structural alignment of the p38α-**2** complex (white, PDB ID: 3IW8) and the crystal structure of Aurora kinase A in complex with a thiazole urea (pink, PDB ID: 3DJ7). Hydrogen bonding interactions are depicted by dotted lines (red for **2** and yellow for the Aurora A inhibitor). (B) Crystal structure of p38α in complex with dasatinib. Electron density maps ($2F_o-F_c$) of p38α (gray) and dasatinib (red) are contoured at 1σ. Dasatinib forms a direct hydrogen bond to the side chain of Thr106, two hydrogen bonds to the backbone of Met109 and a water-mediated hydrogen bond to Lys53. The electron density of Phe169 is not clearly defined indicating the mobility of the DFG-motif. (For interpretation of the references to colour in this figure legend, the reader is referred to the web version of this article.)

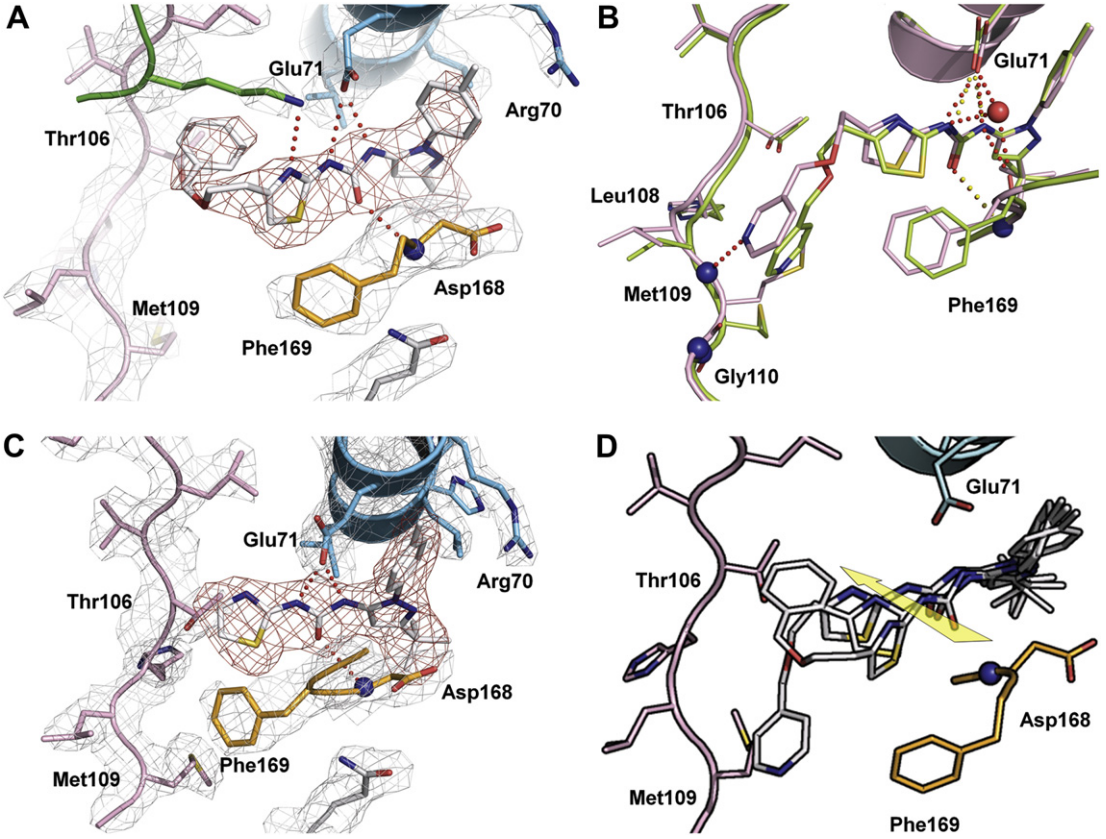

Fig. 3. Crystal structure of wild type p38α in complex with **16a** (A). Electron density maps ($2F_o-F_c$) of p38α (gray) and **16a** (red) are contoured at 1σ. (B) Structural alignment of the p38α-**16c** (pink) and p38α-**16i** (green) complexes. **16i** forms a hydrogen bond (red dots) to the Met109 backbone and a strong network of hydrogen bonds between the urea moiety, Glu71 and Asp168. In contrast, **16c** solely forms hydrogen bonds with Glu71 and Asp168 (yellow dots). Interestingly, a peptide flip of the Met109-Gly110 bond can be observed in the p38α-**16c** complex, although the inhibitor does not form a hydrogen bond to the hinge region. (C) Crystal structure of wild type p38α in complex with **18a**. Electron density maps ($2F_o-F_c$) of p38α (gray) and **18a** (red) are contoured at 1σ. (D) Structural alignment of p38α-crystal structures in complex with **16a**, **16c** or **18a**. The shift of the thiazole core toward the hydrophobic back pocket and the associated reorientation of the urea moiety are shown. (For interpretation of the references to colour in this figure legend, the reader is referred to the web version of this article.)

Interestingly, although **16c** does not form a proper hinge contact it induces a group 2 peptide flip of the Met109-Gly110 bond which has previously been described for p38α [23]. Moreover, reduced electron density in the crystal structure suggests that there is some residual mobility of the pyridine-4-methoxy-ethyl linker of **16c** (Fig. 3). In contrast, the meta-pyridine of **16i** nicely forms a hydrogen bond with the backbone of Met109. Ironically, creation of this hydrogen bond effectively reduces the flexibility of the linker at the expense of entropy, which may explain the lower affinity of **16i** (Fig. 3).

These findings guided further synthetic optimization to avoid the highly flexible linker moiety. Removal of this group resulted in **18a** with a 3-fold higher K_D-value due to the loss of hydrophobic interactions within the hydrophobic back pocket when compared to **16a**. However, analysis of its complex crystal structure confirms that deletion of this flexible group at the same time leads to a more optimal orientation of the thiazole urea pharmacophore, as observed for **16c** and **16i** (Fig. 3), and might explain the rather moderate loss of binding affinity.

Based on these observations and in order to further increase the binding affinity, we incorporated polar groups onto the pyrazole-phenyl ring in an attempt to create hydrogen bonding interactions with the side chain of Arg70 of helix C and to extend the inhibitors within the allosteric pocket. Replacement of the *para* methyl group with an acetic acid moiety (**16e**) resulted in an increased affinity. Similar modification at the *meta* position (**16f**) was less favored. Co-crystallization of **16e** with p38α confirmed the expected binding mode (similar to **16a**) and revealed the formation of an additional hydrogen bond with the side chain of Arg70, thereby explaining the improved affinity (Fig. 4). Although the overall binding mode remains identical to that displayed by **16a**, the novel interaction at the rim of the allosteric pocket further induces a 90° flip of the benzyl-ring which slightly improves the spatial arrangement of this ligand-part (Fig. 4).

Our insights into the binding mode of **18a** and **10e** then led us to speculate that the further addition of the *para* acid functionality to **18a** would result in an even more potent type III inhibitor which forms a novel, crucial hydrogen bond within the allosteric pocket and circumvents the distorted conformation of the central thiazole-urea entity. Finally, we thus synthesized compound **18c** which displayed a 70-fold higher affinity than the hit compound **2** and a 5-fold higher affinity than its closest analog **18a**. Co-crystallization of **18c** in complex with p38α revealed the expected polar interaction of the acid with Arg70, as well as the relaxation of the thiazole-urea moiety (Fig. 4). These interactions are further stabilized by the coordination of three water molecules that form a hydrogen bond network between Asp168, Arg70, the carboxylic acid functionality and the N2 nitrogen atom of the pyrazole. Of interest is that despite the introduction of this additional group, the binding mode of **18c** is isostructural to **18a**.

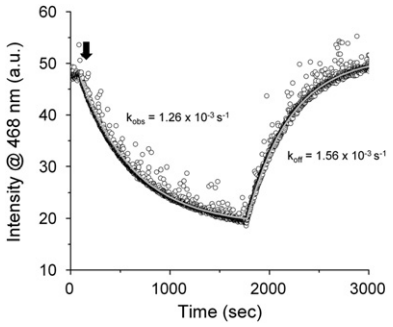

Fig. 5. Real-time binding-measurements for the DFG-out binder **18c**. A single dose of **18c** (500 nM) was added to acrylodan-labeled p38α (50 nM). The fluorescence decay allowed to measure binding (k_{obs}) of the type III inhibitor. Then unlabeled p38α (1 μM) was added to cause dissociation which was fit to a first-order function and allowed k_{off} to be determined.

5. Discussion

Although protein kinases are one of the most investigated targets in drug discovery research, inhibitor selectivity, specificity and acquired drug resistance remain major challenges in kinase inhibitor research [24]. The development of inhibitors that bind to less conserved sites and stabilize kinases in their inactive conformations might overcome these limitations [5,25,26]. We present the promising thiazole-urea scaffold as a starting point for the development of potent p38α inhibitors which extend into the so called allosteric site. In a structure-guided approach we designed and synthesized a focused collection of type II and type III inhibitors. Moreover, the improved type III inhibitors showed excellent inhibition of the enzymatic activity of p38α. We utilized structure-based approaches and SAR analysis to investigate the predicted flexibility of the scaffold and the possibility of extending the binding interactions within the allosteric back pocket. We were able to confirm our hypotheses by determining K_D- and IC_{50}-values,

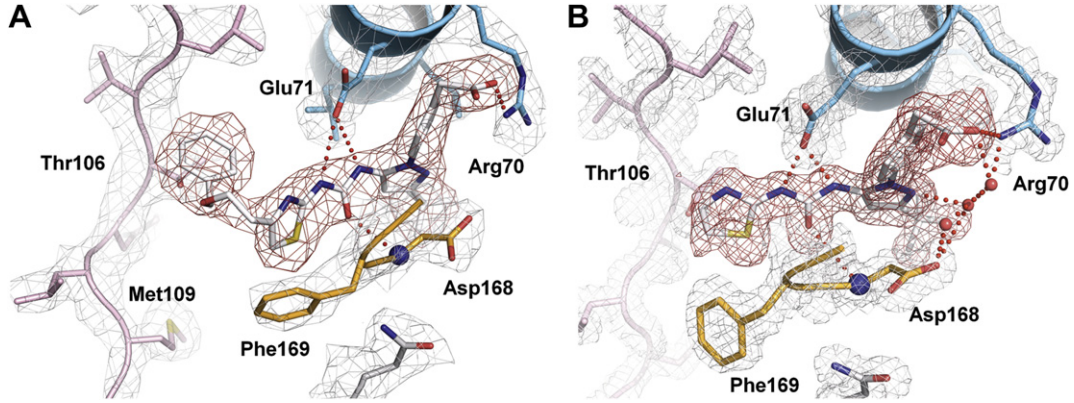

Fig. 4. Crystal structures of p38α in complex with (A) **16e** and (B) **18c**. Electron density maps ($2F_o-F_c$) of p38α (gray) and **16e** and **18c** (red) are contoured at 1σ. Both inhibitors bind to the DFG-out conformation of p38α and are situated within the cleft between the kinase's N- and C-lobe. In addition to the conserved hydrogen bonds between the urea pharmacophore and Glu71 and Asp168, both inhibitors form a hydrogen bond to the side chain of Arg70 of helix C. (For interpretation of the references to colour in this figure legend, the reader is referred to the web version of this article.)

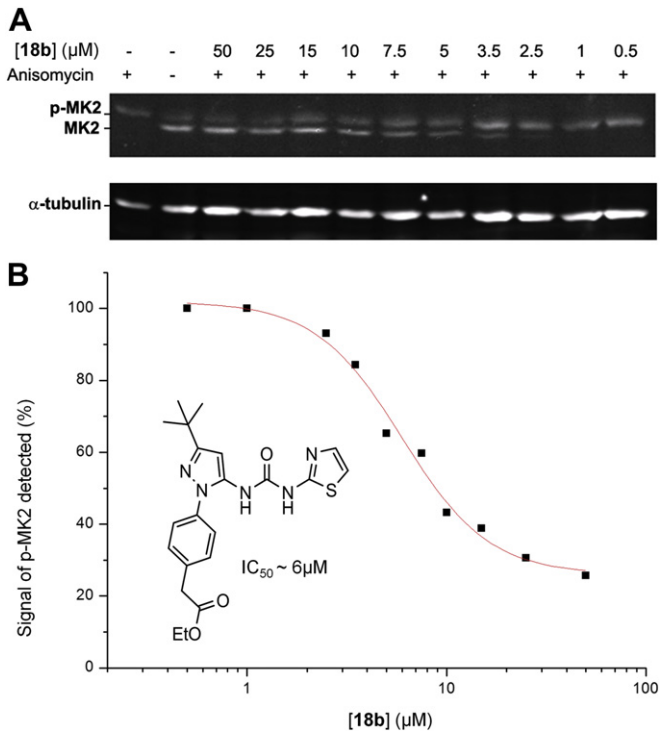

Fig. 6. Dose dependent reduction of MK2 phosphorylation by **18b**. HeLa cells were treated for 2 h with **18b** at 10 different concentrations or vehicle (DMSO) and then stimulated with anisomycin (10 μg/mL) for 30 min. (A) Cells were lysed and blotted for MK2 and phosphorylated MK2 (pMK2) (pT334). The levels of pMK2 are reduced at higher inhibitor concentrations. (B) The blots were scanned using an Odyssey Infrared Scanner and the signals of MK2 and pMK2 were calculated as described in the experimental section. The concentration dependent inhibition of MK2-phosphorylation is demonstrated and reveals a cellular IC_{50} of 6 μM.

and using protein X-ray crystallography. Our initial intention of incorporating polar atoms into the benzyl-ring of the thiazole substituent resulted in type II inhibitors with moderate binding affinities to p38α. This can be attributed to the entropic penalty resulting from the newly formed hydrogen bond to the hinge region which is accompanied with reduced flexibility of the tail moiety. Furthermore, the loss of hydrophobic interactions within the hydrophobic pocket behind the gatekeeper residue further decreases binding affinity. A similar effect was also observed for the phenyl-derivative of BIRB-796, 1-(3-*tert*-butyl-1-*p*-tolyl-1*H*-pyrazol-5-yl)-3-[4-(2-morpholinoethoxy)phenyl]urea, which displayed a much lower potency than its parent type III precursors and BIRB-796 itself [7,27]. We then turned our attention to the development of type III inhibitors. The addition of acetic acid functionality to the pyrazole-phenyl ring led to the formation of a network of hydrogen bonding interactions within the allosteric pocket and was crucial for higher binding affinities. At the same time, the removal of the 4-benzyloxy-ethyl moiety enabled the thiazole-urea pharmacophore to adopt a more optimal binding geometry which was essential to restore the ideal orientation of this entity and allow the formation of strong hydrogen bonds with the backbone of the DFG-motif (Asp168) and the side chain of Glu71 of helix C. The presented attempt of growing inhibitors into the allosteric pocket might represent an attractive approach to develop inhibitors with advantageous pharmacological profiles. While targeting the kinase outside the ATP site and stabilizing the inactive conformation, inhibitor potencies can be conserved through the formation of novel interactions within the allosteric site. This approach might stimulate further inhibitor development based on the presented inhibitor scaffold and its unique binding mode in p38α.

6. Conclusion

In conclusion, we have developed potent p38α inhibitors guided by structure-based design. We improved the affinity of the previously identified hit structures by 70-fold while exploiting the allosteric pocket of p38α and can explain these improved affinities using protein X-ray crystallography. Furthermore, we showed that **18c** can be a useful lead structure for further inhibitor development by generating new interactions within the allosteric pocket outside the ATP site. Additionally, these results highlight the strength of the FLiK assay technology that not only allows the detection of low affinity binders to inactive kinases in screening scenarios, but also can serve as a powerful tool in optimizing and analyzing binding characteristics of compounds of interest.

7. Experimental protocols

7.1. Chemistry

Unless otherwise noted, all reagents and solvents were purchased from Acros, Fluka, Sigma, Aldrich or Merck and used without further purification. Dry solvents were purchased as anhydrous reagents from commercial suppliers. ^{1}H and ^{13}C NMR spectra were recorded on a Varian Mercury 400, Bruker Avance DRX 400, Bruker DRX 500 or Varian Inova 600 spectrometer. ^{1}H NMR spectroscopic chemical shifts are reported in δ (ppm) as s (singlet), d (doublet), dd (doublet of doublet), t (triplet), q (quartet), m (multiplet) and bs (broad singlet), and are referenced to the residual solvent signal: $CDCl_3$ (7.26), CD_3OD (4.87) and, DMSO-d_6 (2.50). ^{13}C NMR spectra are referenced to the residual solvent signal: $CDCl_3$ (77.0), CD_3OD (21.4), DMSO-d_6 (39.0). All final compounds were purified to >95% purity, as determined by high-performance liquid chromatography (HPLC). Purities were measured using an Agilent 1200 Series HPLC system with UV detection at 210 nm (System: Agilent Eclipse XDB-C18 4.6 × 150 mm, 5 μM, 10–100% CH_3CN in H_2O, with 0.1% TFA, for 15 min at 1.0 mL/min). High resolution electrospray ionization mass spectra (ESI-FTMS) were recorded on a Thermo LTQ Orbitrap (high resolution mass spectrometer from Thermo Electron) coupled to an 'Accela' HPLC System supplied with a 'Hypersil GOLD' column (Thermo Electron). Analytical TLC was carried out on Merck 60 F245 aluminum-backed silica gel plates. Compounds were purified by column chromatography using Baker silica gel (40–70 μm particle size). Preparative HPLC was conducted on a Varian HPLC system (Pro Star 215) with a VP 250/21 Nucleosil C18 PPN column from Macherey–Nagel and monitored by UV at $\lambda = 254$ nm. Microwave-assisted reactions were carried out with a 'Discover' system from CEM Corporation.

7.1.1. *tert*-Butyl 4-(2-hydroxyethyl)-1,3-thiazol-2-ylcarbamate (**7**)

Boc_2O (4.3 g, 20 mmol) was added portion-wise over 5 min, to ethyl (2-amino-1,3-thiazol-4-yl)acetate (3.72 g, 20 mmol) dissolved in cold (0 °C, ice bath) THF (100 mL). NEt_3 (5.6 mL, 40 mmol) was then added drop-wise by syringe, followed by a catalytic amount of DMAP (0.1 g) [28]. The reaction was then stirred at rt for 18 h, after which EtOAc (200 mL) was added. The organic phase was sequentially washed with aq. HCl (1 N, 300 mL) and saturated brine (2 × 200 mL), after which it was dried ($MgSO_4$). The organic solution was filtered through a short silica plug after which the organic solvent removed *in vacuo*. The reaction was performed twice and the combined residues were then purified by column chromatography on flash silica (eluent: 20% EtOAc/cyclohexane) to afford the desired product ethyl {2-[(*tert*-butoxycarbonyl)amino]-1,3-thiazol-4-yl}acetate **6** (5.6 g, 49%) which was used directly in the next reaction. $NaBH_4$ (2.2 g, 60 mmol) was then added portion-wise over 5 min, to **6** (5.6 g, 20 mmol) dissolved in cold (0 °C, ice bath) EtOH

(90 mL) [29]. The reaction was then stirred at rt for 18 h, after which the solvent was removed under reduced pressure. EtOAc (200 mL) was then added to the remaining residue and the organic phase was subsequently washed with saturated brine (2 × 50 mL), after which it was dried ($MgSO_4$). The remaining residue was then purified by column chromatography on flash silica (eluent: EtOAc) to afford the desired product **7** (2.18 g, 47%): ^{1}H NMR (400 MHz, $CDCl_3$) δ 10.09 (bs, 1H), 6.52 (s, 1H), 3.89 (t, J = 5.7 Hz, 2H), 2.87 (t, J = 5.7 Hz, 2H), 1.53 (s, 9H); ^{13}C NMR (101 MHz, $CDCl_3$) δ 160.5, 152.4, 149.2, 107.3, 82.2, 61.9, 33.3, 28.2. HRMS (ESI-MS) Calc.: 335.14239 for $C_{17}H_{23}N_2O_3S$ [M + H$^+$], Found: 335.14247.

7.1.2. General procedure for the alkylation of tert-butyl 4-(2-hydroxyethyl)-1,3-thiazol-2-ylcarbamate

NaH (60% in oil, 3 mol equiv.) was added in one portion to the alcohol **7** dissolved in dry THF (~5 mL/mmol) and the reaction mixture was stirred for 10 min under an Ar atmosphere. The substituted benzyl bromide (1–1.2 mol equiv.) was then added and the reaction mixture was stirred at rt for a period of 48–72 h. H_2O (10–20 mL) was then added and the THF removed under reduced pressure. The remaining aqueous liquid was extracted with EtOAc or CH_2Cl_2 (3 × 20 mL), which was combined, washed with brine, dried over $MgSO_4$ and removed *in vacuo*. The alkylated product was then obtained after column chromatography with flash silica. The following compounds were synthesized using this procedure.

*7.1.2.1. tert-Butyl 4-[2-(benzyloxy)ethyl]-1,3-thiazol-2-ylcarbamate (**23a**).* Prepared as described above in the general procedure using (**7**) (1.0 g, 4.1 mmol), NaH (0.49 g, 12.2 mmol) and benzyl bromide (0.49 mL, 4.1 mmol) in THF (20 mL). The product **23a** (1.05 g, 76%) was obtained as a clear oil after chromatography (eluent: 10% EtOAc/cyclohexane): ^{1}H NMR (400 MHz, $CDCl_3$) δ 9.94 (bs, 1H), 7.38–7.19 (m, 5H), 6.57 (s, 1H), 4.52 (s, 2H), 3.75 (t, J = 6.8 Hz, 2H), 3.02 (t, J = 6.8 Hz, 2H), 1.54 (s, 9H); ^{13}C NMR (101 MHz, CD_3OD) δ 161.5, 154.4, 149.8, 139.6, 129.3, 128.8, 128.6, 108.9, 82.8, 73.8, 70.1, 32.8, 28.5. ESI: 335 ([M + H$^+$], 100%), 278 (85); HRMS (ESI-MS) Calc.: 335.14239 for $C_{17}H_{23}N_2O_3S$ [M + H$^+$], Found: 335.14247.

*7.1.2.2. tert-Butyl 4-{2-[(4-fluorobenzyl)oxy]ethyl}-1,3-thiazol-2-ylcarbamate (**23b**).* Prepared as described above in the general procedure using **7** (0.20 g, 0.82 mmol), NaH (0.098 g, 2.5 mmol) and 4-fluorobenzyl bromide (0.11 mL, 0.90 mmol) in THF (4 mL). The product **23b** (0.16 g, 55%) was obtained as a clear oil after chromatography (eluent: 30% EtOAc/cyclohexane), in addition to a small amount of slightly contaminated product (0.044 g, 15%): ^{1}H NMR (400 MHz, $CDCl_3$) δ 10.88 (bs, 1H), 7.15–7.12 (m, 2H), 6.85–6.89 (m, 2H), 6.47 (s, 1H), 4.36 (s, 2H), 3.63 (t, J = 6.9 Hz, 2H), 2.96 (t, J = 6.9 Hz, 2H), 1.43 (s, 9H); ^{13}C NMR (101 MHz, $CDCl_3$) δ 162.1 ($^1J_{C-F}$ = 249.1 Hz, 2C), 160.8, 152.6, 148.4, 133.9, 129.2 ($^3J_{C-F}$ = 8.0 Hz, 2C), 115.0 ($^2J_{C-F}$ = 21.0 Hz, 2C), 107.3, 82.3, 72.1, 68.9, 31.6, 28.1; ESI: 375 (40%), 353 ([M + H$^+$], 100), 296 (45); HRMS (ESI-MS) Calc.: 353.13297 for $C_{17}H_{22}FN_2O_3S$ [M + H$^+$], Found: 353.13307.

*7.1.2.3. tert-Butyl 4-[2-(4-pyridinylmethoxy)ethyl]-1,3-thiazol-2-ylcarbamate (**23c**).* Prepared as described above in the general procedure using **7** (0.20 g, 0.82 mmol), NaH (0.13 g, 4.0 mmol) and 4-(bromomethyl)pyridine hydrobromide (0.23 g, 0.90 mmol) in THF (4 mL). The product **23c** (0.13 g, 50%) was obtained as a clear oil after column chromatography (eluent: EtOAc): ^{1}H NMR (400 MHz, $CDCl_3$) δ 8.50 (d, J = 6.0 Hz, 2H), 7.16 (d, J = 6.0 Hz, 2H), 6.55 (s, 1H), 4.49 (s, 2H), 3.75 (t, J = 6.8 Hz, 2H), 3.03 (t, J = 6.8 Hz, 2H), 1.50 (s, 9H); ^{13}C NMR (101 MHz, $CDCl_3$) δ 160.6, 152.6, 149.8, 148.2, 147.6, 121.5, 107.5, 82.3, 71.0, 69.6, 31.7, 28.2; ESI: 670 (2[M + H$^+$], 50%), 336 (100), 235 (30); HRMS (ESI-MS) Calc.: 336.13764 for $C_{16}H_{22}N_3O_3S$ [M + H$^+$], Found: 336.13772.

7.1.3. General procedure for the removal of the Boc group

Hydrochloric acid in dioxane (4 M) was added to the *tert*-butyl carbamate and the reaction was stirred at rt under an Ar atmosphere for 14–96 h. If required, a small amount of MeOH was added to aid solubility of the starting material. The solvent was removed under reduced vacuum and the resulting residue was subjected to a high vacuum overnight. All compounds were isolated as opaque oils or white semi-solids in quantitative yields. NMR spectroscopy showed that the resulting products, which were isolated as their respective HCl salts, to be of sufficient purity to be utilized directly in the subsequent coupling reactions. The following compounds were synthesized using this procedure.

*7.1.3.1. 4-[2-(Benzyloxy)ethyl]-1,3-thiazol-2-aminium chloride (**8a**).* Prepared as described above in the general procedure using **23a** (0.30 g, 0.90 mmol), HCl in dioxane (4 M, 4 mL) and MeOH (2 mL). Removal of the solvent then afforded **8a** as a white semi-solid (0.24 g, quantitative): ^{1}H NMR (400 MHz, CD_3OD) δ 7.31–7.25 (m, 5H), 6.54 (br s, 1H), 4.54 (s, 2H), 3.70 (t, J = 6.3 Hz, 2H), 2.85 (t, J = 6.3 Hz, 2H); ^{13}C NMR (101 MHz, CD_3OD) δ 139.5, 139.3, 129.5, 129.0, 128.9, 104.0, 74.0, 68.4, 68.1, 29.5; ESI: 235 ([M + H$^+$], 100%), 91 (20); HRMS (ESI-MS) Calc.: 235.08996 for $C_{12}H_{15}N_2OS$ [M + H$^+$], Found: 235.08982.

*7.1.3.2. 4-{2-[(4-Fluorobenzyl)oxy]ethyl}-1,3-thiazol-2-aminium chloride (**8b**).* Prepared as described above in the general procedure using **23b** (0.15 g, 0.43 mmol), HCl in dioxane (4 M, 10 mL). Removal of the solvent then afforded **8a** as a white semi-solid (0.12 g, quantitative): ^{1}H NMR (400 MHz, CD_3OD) δ 7.34–7.31 (m, 2H), 7.07–7.02 (m, 2H), 6.55 (s, 1H), 4.51 (s, 2H), 3.70 (t, J = 6.3 Hz, 2H), 2.85 (t, J = 6.3 Hz, 2H); ^{13}C NMR (101 MHz, CD_3OD) δ 171.9, 163.7 ($^1J_{C-F}$ = 245.0 Hz, 2C), 139.3, 135.4, 130.9 ($^3J_{C-F}$ = 8.0 Hz, 2C), 116.0 ($^2J_{C-F}$ = 23.0 Hz, 2C), 104.0, 73.1, 68.4, 29.5; ESI: 504 (10%), 253 ([M + H$^+$], 100). HRMS (ESI-MS) Calc.: 253.08054 for $C_{12}H_{14}FN_2OS$ [M + H$^+$], Found: 253.08060.

*7.1.3.3. 4-[2-(4-Pyridinylmethoxy)ethyl]-1,3-thiazol-2-aminium chloride (**8c**).* Prepared as described above in the general procedure using **23c** (0.13 g, 0.39 mmol), HCl in dioxane (4 M, 10 mL) and MeOH (2 mL). Removal of the solvent then afforded **8c** as a white semi-solid (0.12 g, quantitative): ^{1}H NMR (400 MHz, CD_3OD) δ 8.85 (d, J = 6.7 Hz, 2H), 8.10 (d, J = 6.7 Hz, 2H), 6.70 (s, 1H), 4.96 (s, 2H), 3.95 (t, J = 6.0 Hz, 2H), 3.02 (t, J = 6.0 Hz, 2H); ^{13}C NMR (101 MHz, CD_3OD) δ 172.0, 162.2, 142.3, 138.3, 125.8, 104.5, 69.9, 68.1, 29.3; ESI: 470 (2[M + H$^+$], 50%), 236 (100); HRMS (ESI-MS) Calc.: 236.08521 for $C_{11}H_{14}N_3OS$ [M + H$^+$], Found: 236.08532.

*7.1.4. Preparation of 1-cyclopropylbut-3-yn-1-one (**12a**)*

To a suspension of NaH (4.2 g, 110 mmol) in THF (15 mL) at 70 °C was added dropwise a solution of methyl cyclopropanecarboxylate **11a** (10 mL, 96 mmol) and anhydrous acetonitrile (6.1 mL, 116 mmol) in THF (10 mL). The mixture was stirred for 16 h at 70 °C, cooled to rt, and diluted with ethyl acetate and aqueous HCl. The organic layer was washed with water and brine and dried over Na_2SO_4. The volatiles were removed *in vacuo* and furnished an orange solid which was then refluxed in petroleum ether and filtered off to give the product as 10.1 g (96%) of an orange solid: ^{1}H NMR (400 MHz, DMSO-d_6) δ 3.59 (s, 2H), 2.11–2.05 (m, 1H), 1.19–1.15 (m, 2H), 1.09–1.04 (m, 2H); ^{13}C NMR (101 MHz, DMSO-d_6) δ 197.82, 114.11, 32.87, 20.33, 13.13.

*7.1.5. Preparation of 3-cyclopentyl-3-oxopropanenitrile (**12b**)*

The compound was synthesized from NaH (1.7 g, 42 mmol), methyl cyclopentanecarboxylate **11b** (5.3 mL, 38 mmol) and anhydrous acetonitrile (2.4 mL, 46 mmol) in THF (20 mL) according

to patent literature [12]. The volatiles were removed *in vacuo* and furnished the product which was used without further purification.

*7.1.6. General procedure for the preparation of (hydrazinylphenyl) acetic acid hydrochlorides **14a**,**b***

Compounds **14a** and **b** were synthesized according to patent literature as follows [12]. To a solution of amino benzoic acid in concentrated HCl, an aqueous solution of $NaNO_2$ was added at 0 °C. The reaction mixture was then stirred for 1h and a solution of $SnCl_2 \times 2H_2O$ in concentrated HCl was then added at 0 °C, and the reaction mixture was stirred for additional 2h at rt before it was extracted with EtOAc (4 × 50 mL). The volatiles were removed *in vacuo* to yield (hydrazinylphenyl)acetic acid hydrochlorides.

*7.1.6.1. 2-(3-(Carboxymethyl)phenyl)hydrazinium chloride (**14a**).* Prepared as described above in the general procedure using *m*-(aminophenyl)acetic acid **13a** (9.8 g, 63 mmol) in concentrated HCl (10 mL), $NaNO_2$ (4.3 g, 63 mmol) in H_2O (10 mL) and $SnCl_2 \times 2H_2O$ (28.4 g, 126 mmol) in concentrated HCl (5 mL). The crude product was obtained as brown oil and was used without further purification.

*7.1.6.2. 2-(4-(Carboxymethyl)phenyl)hydrazinium chloride (**14b**).* Prepared as described above in the general procedure using *p*-(aminophenyl)acetic acid **13b** (9.8 g, 63 mmol) in concentrated HCl (10 mL), $NaNO_2$ (4.3 g, 63 mmol) in H_2O (10 mL) and $SnCl_2 \times 2H_2O$ (28.4 g, 126 mmol) in concentrated HCl (5 mL). The crude product was obtained as a brown solid and was used without further purification.

*7.1.7. General procedure for the preparation of carbamates **15b–f***

Hydrazine hydrochloride **14a** or **b** was refluxed with nitrile **12a**,**b** or **c** in EtOH overnight. The reaction solution was evaporated *in vacuo* to furnish the corresponding pyrazolo amine, which was used without further purification. A mixture of the pyrazolo amine, H_2O, EtOAc and NaOH was stirred at 0° for 30 min. Then 2,2,2-richloroethyl chloroformate was added drop-wise. After a further 30 min the ice bath was removed and the reaction mixture was stirred at rt for an additional 2 h. The organic layer was separated from the aqueous layer which was extracted with EtOAc (4 × 10 mL). The combined organic layers were washed with brine twice, dried over Na_2SO_4 and evaporated *in vacuo*. The purification of each compound is described separately for every compound.

*7.1.7.1. Ethyl [3-(3-cyclopropyl-5-{[(2,2,2-trichloroethoxy)carbonyl] amino}-1H-pyrazol-1-yl)phenyl]acetate (**15b**).* Prepared as described above using **14a** (4.1 g, 20 mmol) and **12a** (2.2 g, 20 mmol) to give ethyl 2-(3-(5-amino-3-cyclopropyl-1*H*-pyrazol-1-yl)phenyl)acetate **24a**. Then **24a** (3.3 g, 10 mmol), 2,2,2-trichloroethyl chloroformate (1.6 mL, 12 mmol), NaOH (0.7 g, 20 mmol), H_2O (10 mL) and EtOAc (15 mL) were combined as described in the general experimental procedure. The volatiles were next evaporated *in vacuo* and The crude residue was purified on silica gel (20% EtOAc/petroleum ether) to yield 0.42 g (9%, 3 steps) of **15b**: ^{1}H NMR (400 MHz, DMSO-d_6) δ 7.46–7.37 (m, 2H), 7.35–7.27 (m, 2H), 7.07 (bs, 1H), 6.19 (s, 1H), 4.78 (s, 2H), 4.14 (q, J = 7.2 Hz, 2H), 3.64 (s, 2H), 1.98–1.89 (m, 1H), 1.24 (t, J = 7.1 Hz, 3H), 0.95–0.89 (m, 2H), 0.80–0.73 (m, 2H); ^{13}C NMR (101 MHz, DMSO-d_6) δ 171.29, 156.30, 155.63, 137.97, 136.22, 135.46, 130.04, 129.40, 126.03, 123.41, 95.00, 94.90, 75.12, 61.39, 41.07, 14.41, 9.74, 8.16; HRMS (ESI-MS) Calc.: 460.05922 for $C_{19}H_{21}O_4N_3^{35}Cl_3$ [M + H$^+$], Found: 460.05880 and calc.: 462.05627 for $C_{19}H_{21}O_4N_3^{35}Cl_2^{37}Cl$ [M + H$^+$], Found: 462.05542.

*7.1.7.2. Ethyl [4-(3-tert-butyl-5-{[(2,2,2-trichloroethoxy)carbonyl] amino}-1H-pyrazol-1-yl)phenyl]acetate (**15c**).* Prepared as described above using **14b** (4.0 g, 20 mmol) and pivaloyl acetonitrile (2.7 g, 20 mmol) to give ethyl 2-(4-(5-amino-3-*tert*-butyl-1*H*-pyrazol-1-yl) phenyl)acetate **24b** which was refluxed in petrol ether to furnish 3.8 g (63%) of an orange solid. Then 2-(4-(5-amino-3-*tert*-butyl-1*H*-pyrazol-1-yl)phenyl)acetate **24b** (2.0 g, 6.6 mmol), 2,2,2-trichloroethyl chloroformate (912 μL, 6.6 mmol), NaOH (0.4 g, 10 mmol), H_2O (10 mL) and EtOAc (10 mL) were combined as described in the general experimental procedure. The crude residue was purified on silica gel (20% EtOAc/petroleum ether) to yield 3.1 g (97%) of **15c**: ^{1}H NMR (400 MHz, DMSO-d_6) δ 7.43–7.34 (m, 4H), 6.98 (bs, 1H), 6.39 (s, 1H), 4.78 (s, 2H), 4.12 (q, J = 7.0 Hz, 2H), 3.63 (s, 2H), 1.31 (s, 9H), 1.24 (t, J = 7.1 Hz, 3H); ^{13}C NMR (101 MHz, DMSO-d_6) δ 171.57, 162.83, 151.29, 137.12, 135.29, 134.74, 131.08, 125.42, 95.66, 95.21, 75.27, 61.56, 41.31, 32.86, 30.67, 14.59; HRMS (ESI-MS) Calc.: 476.09052 for $C_{20}H_{25}O_4N_3^{35}Cl_3$ [M + H$^+$], Found: 476.09025 and calc.: 478.08757 for $C_{21}H_{25}O_4N_3^{35}Cl_2^{37}Cl$ [M + H$^+$], Found: 478.08683.

*7.1.7.3. Ethyl [3-(3-tert-butyl-5-{[(2,2,2-trichloroethoxy)carbonyl] amino}-1H-pyrazol-1-yl)phenyl]acetate (**15d**).* Prepared as described above using **14a** (4.0 g, 20 mmol) and pivaloyl acetonitrile (2.7 g, 20 mmol) to give ethyl 2-(3-(5-amino-3-*tert*-butyl-1*H*-pyrazol-1-yl) phenyl)acetate **24c** which was used without further purification. Then **24c** (6.0 g, 20 mmol), 2,2,2-trichloroethyl chloroformate (3 mL, 20 mmol), NaOH (1.6 g, 40 mmol), H_2O (20 mL) and EtOAc (20 mL) were combined as described in the general experimental procedure. The crude residue was recrystallized from petroleum ether/EtOAc to yield 3.55 g (37%) of **15d**: ^{1}H NMR (400 MHz, DMSO-d_6) δ 7.46–7.38 (m, 2H), 7.35 (d, J = 7.8 Hz, 1H), 7.29 (d, J = 7.5 Hz, 1H), 6.97 (bs, 1H), 6.40 (s, 1H), 4.79 (2H), 4.14 (q, 7.1 Hz, 2H), 3.64 (s, 2H), 1.32 (s, 9H), 1.24 (t, 3H); ^{13}C NMR (101 MHz, DMSO-d_6) δ 171.24, 162.73, 151.05, 138.18, 136.19, 135.01, 130.01, 129.29, 126.11, 123.50, 95.41, 95.03, 75.07, 61.35, 41.12, 32.65, 30.48, 14.40; HRMS (ESI-MS) Calc.: 476.09052 for $C_{20}H_{25}O_4N_3^{35}Cl_3$ [M + H$^+$], Found: 476.09031 and calc.: 478.08757 for $C_{21}H_{25}O_4N_3^{35}Cl_2^{37}Cl$ [M + H$^+$], Found: 478.08687.

*7.1.7.4. Ethyl [3-(3-cyclopentyl-5-{[(2,2,2-trichloroethoxy)carbonyl] amino}-1H-pyrazol-1-yl)phenyl]acetate (**15e**).* Prepared as described above using **14a** (3.8 g, 19 mmol) and **12b** (2.6 g, 19 mmol) to give ethyl 2-(3-(5-amino-3-cyclopentyl-1*H*-pyrazol-1-yl)phenyl)acetate **24d** which was used without further purification. Then **24d** (6.2 g, 20 mmol), 2,2,2-trichloroethyl chloroformate (2.7 mL, 20 mmol), NaOH (1.6 g, 40 mmol), H_2O (20 mL) and EtOAc (20 mL) were combined as described in the general experimental procedure. The crude residue was purified on silica gel (20% EtOAc/petroleum ether) to yield 0.48 mg (5%) of **15e**: ^{1}H NMR (400 MHz, DMSO-d_6) δ 7.45–7.37 (m, 2H), 7.34 (d, J = 7.9 Hz, 1H), 7.29 (d, J = 7.5 Hz, 1H), 7.08 (bs, 1H), 6.36 (s, 1H), 4.78 (s, 2H), 4.13 (q, J = 7.1 Hz, 2H), 3.64 (s, 2H), 3.07 (m, 1H), 2.09–2.00 (m, 2H), 1.79–1.22 (m, 6H), 1.24 (t, J = 7.1 Hz, 3H); ^{13}C NMR (101 MHz, DMSO-d_6) δ 171.30, 170.75, 158.52, 151.07, 138.04, 136.16, 129.98, 129.32, 126.05, 123.42, 96.11, 95.03, 75.11, 61.37, 41.07, 39.58, 33.43, 25.65, 14.39; HRMS (ESI-MS) Calc.: 488.09052 for $C_{21}H_{25}O_4N_3^{35}Cl_3$ [M + H$^+$], Found: 488.09024 and calc.: 490.08757 for $C_{21}H_{25}O_4N_3^{35}Cl_2^{37}Cl$ [M + H$^+$], Found: 490.08689.

*7.1.7.5. Ethyl [4-(3-cyclopentyl-5-{[(2,2,2-trichloroethoxy)carbonyl] amino}-1H-pyrazol-1-yl)phenyl]acetate (**15f**).* Prepared as described above using **14b** (3.8 g, 19 mmol) and **12b** (2.6 g, 19 mmol) to give ethyl 2-(4-(5-amino-3-cyclopentyl-1*H*-pyrazol-1-yl)phenyl)acetate **24b** which was used without further purification. Then **24b** (1.0 g, 3.2 mmol), 2,2,2-trichloroethyl chloroformate (0.44 mL, 3.19 mmol), NaOH (0.3 g, 10 mmol), H_2O (10 mL) and EtOAc (10 mL) were combined as described in the general experimental procedure. The crude residue was purified on silica gel (20% EtOAc/petroleum ether) to yield 0.84 g (55%) of **15f**: ^{1}H NMR (400 MHz, DMSO-d_6) δ 7.41–7.34 (m, 4H), 7.03 (bs, 1H), 6.33 (s, 1H), 4.78 (s, 2H), 4.14 (q,

J = 7.1 Hz, 2H), 3.63 (s, 2H), 3.09–3.00 (m, 1H), 2.07–1.99 (m, 2H), 1.79–1.58 (m, 6H), 1.24 (t, J = 7.1 Hz, 3H); ^{13}C NMR (101 MHz, DMSO-d_6) δ 171.35, 158.42, 151.15, 136.94, 135.21, 134.44, 130.82, 125.02, 96.24, 95.01, 75.06, 61.33, 41.08, 39.58, 33.40, 25.64, 14.37; HRMS (ESI-MS) Calc.: 488.09052 for $C_{21}H_{25}O_4N_3^{35}Cl_3$ [M + H$^+$], Found: 488.09016 and calc.: 490.08757 for $C_{21}H_{25}O_4N_3^{35}Cl_2^{37}Cl$ [M + H$^+$], Found: 490.08676.

*7.1.8. N-{4-[2-(Benzyloxy)ethyl]-1,3-thiazol-2-yl}-N′-[4-chloro-3-(trifluoromethyl)phenyl]-urea (**20**)*

A mixture of **8a** (31 mg, 0.11 mmol), 1-chloro-4-isocyanato-2-(trifluoromethyl)benzene **19** (25 mg, 0.11 mmol) and DIPEA (58 μL, 0.34 mmol) in anhydrous DCM (2 mL) was stirred at rt for 12 h. Removal of the volatiles *in vacuo* provided the crude residue which was purified on silica gel (1–1.5% MeOH/DCM). The product was obtained as 14 mg (36%) of a white solid: ^{1}H NMR (400 MHz, DMSO-d_6) δ 10.88 (bs, 1H), 9.43 (s, 1H), 8.11 (d, J = 2.3 Hz, 1H), 7.72 (dd, J = 8.8, 2.1 Hz, 1H), 7.63 (d, J = 8.8 Hz, 1H), 7.37–7.24 (m, 5H), 6.75 (s, 1H), 4.49 (s, 2H), 3.70 (t, J = 6.8 Hz, 2H), 2.85 (t, J = 6.7 Hz, 2H); ^{13}C NMR (101 MHz, DMSO-d_6) δ 138.65, 138.49, 132.10, 128.26, 128.07, 127.52, 127.42, 126.92, 126.74 ($^2J_{C-F}$ = 30.6 Hz), 126.43, 123.52, 123.06, 122.74 ($^3J_{C-F}$ = 272.1 Hz), 117.18 ($^1J_{C-F}$ = 5.5 Hz), 107.26, 71.79, 68.42, 31.11; HRMS (ESI-MS) Calc.: 456.07549 for $C_{20}H_{18}O_2N_3^{35}ClF_3S$ [M + H$^+$], Found: 456.07498 and calc.: 458.07254 for $C_{20}H_{18}O_2N_3^{37}ClF_3S$ [M + H$^+$], Found: 458.07212.

*7.1.9. N-[3-tert-Butyl-1-(4-methylphenyl)-1H-pyrazol-5-yl]-N′-(1,3-thiazol-2-yl)urea (**18a**)*

Thiazol-2-amine **17** (13 mg, 0.12 mmol), **15a** (50 mg, 0.12 mmol) and DIPEA (62 μL, 0.36 mmol) were dissolved in anhydrous DMSO (2 mL) and irradiated for 30 min at 100 °C in the microwave (100 W). After cooling to rt the mixture was portioned between EtOAc and H_2O. The aqueous layer was extracted with EtOAc (3 × 10 mL). The combined organic layer was then washed with brine and H_2O, dried over Na_2SO_4 and evaporated *in vacuo*. The crude residue was purified using silica gel chromatography (1–2% MeOH/CH_2Cl_2) yielding 25 mg (59%) of **18a**: ^{1}H NMR (400 MHz, DMSO-d_6) δ 10.88 (bs, 1H), 8.86 (bs, 1H), 7.39 (d, J = 8.4 Hz, 2H), 7.36–7.32 (m, 3H), 7.12 (d, J = 3.5 Hz, 1H), 6.41 (s, 1H), 2.37 (s, 3H), 1.28 (s, 9H); ^{13}C NMR (101 MHz, DMSO-d_6) δ 160.66, 159.30, 150.81, 150.56, 137.06, 136.28, 135.70, 129.76, 124.52, 112.68, 94.82, 32.06, 30.21, 20.63. HRMS (ESI-MS) Calc.: 356.15396 for $C_{18}H_{22}ON_5S$ [M + H$^+$], Found: 356.15405.

*7.1.10. [4-(3-tert-Butyl-5-{[(1,3-thiazol-2-ylamino)carbonyl]amino}-1H-pyrazol-1-yl)phenyl]-acetic acid (**18c**)*

Thiazol-2-amine **17** (43 mg, 0.31 mmol), **15c** (150 mg, 0.31 mmol) and DIPEA (185 μL, 0.108 mmol) were dissolved in anhydrous DMSO (2 mL) and irradiated at 60 °C overnight. After cooling to rt the mixture was portioned between EtOAc and H_2O. The aqueous layer was then extracted with EtOAc (3 × 10 mL). The combined organic layer was washed with brine and H_2O, dried over Na_2SO_4 and evaporated *in vacuo*. The crude residue was subsequently divided into two fractions: a) 50 mg of the crude residue were purified using silica gel chromatography (0–1% MeOH/CH_2Cl_2) to afford **18b** (12 mg). b) The remaining crude residue was redissolved in MeOH/H_2O (1:1, 2 mL) and an aqueous solution of LiOH (2 eq., 2 mL) was added. The reaction mixture was stirred at rt for 30 min and then diluted with EtOAc (5 mL) and diluted formic acid (2 mL). The organic layer was dried over Na_2SO_4, before the volatiles were removed *in vacuo*. The crude product was then purified using preparative HPLC (MeCN/H_2O with 0.1% TFA) and a subsequent step using silica gel chromatography (1–2% MeOH/CH_2Cl_2) yielding 15 mg (12%) of **18c**: ^{1}H NMR (400 MHz, DMSO-d_6) δ 9.04 (bs, 1H), 7.46 (d, J = 8.5 Hz, 2H), 7.42 (d, J = 8.5 Hz, 2H), 7.34 (d, J = 3.6 Hz, 1H), 7.11 (d, J = 3.6 Hz, 1H), 6.43 (s, 1H), 3.66 (s, 2H), 1.28 (s, 9H); ^{13}C NMR (101 MHz, DMSO-d_6) δ 172.58, 160.88, 159.52, 150.77, 137.33, 136.75, 136.36, 134.53, 130.35, 124.30, 112.64, 95.03, 40.23, 32.09, 30.20. HRMS (ESI-MS) Calc.: 400.143709 for $C_{19}H_{22}O_3N_5S$ [M + H$^+$], Found: 400.14307.

*7.1.11. Ethyl [4-(3-tert-butyl-5-{[(1,3-thiazol-2-ylamino)carbonyl]amino}-1H-pyrazol-1-yl)phenyl]acetate **18b***

^{1}H NMR (500 MHz, DMSO-d_6) δ 10.85 (s, 1H), 8.94 (s, 1H), 7.48 (d, J = 8.5 Hz, 2H), 7.43 (d, J = 8.4 Hz, 2H), 7.33 (d, J = 3.5 Hz, 1H), 7.12 (s, 1H), 6.43 (s, 1H), 4.11 (q, J = 7.1 Hz, 2H), 3.75 (s, 2H), 1.28 (s, 9H), 1.20 (*t*, J = 7.1 Hz, 3H); ^{13}C NMR (125 MHz, DMSO-d_6) δ 173.21, 170.90, 164.04, 151.69, 150.18, 138.57, 138.25, 136.83, 131.82, 127.26, 113.66, 96.17, 62.25, 41.66, 33.52, 30.88, 14.62. HRMS (ESI-MS) Calc.: 428.17509 for $C_{21}H_{26}O_3N_5S$ [M + H$^+$], Found :428.17455.

*7.1.12. N-{4-[2-(Benzyloxy)ethyl]-1,3-thiazol-2-yl}-3-fluoro-5-(4-morpholinyl)benzamide (**22**)*

3-Fluoro-5-morpholinobenzoic acid **21** (synthesized according to patent literature) [30] (50 mg, 0.22 mmol), **6a** (40 mg, 0.15 mmol), HBTU (69 mg, 0.30 mg) and DIPEA (101 μL, 0.59 mmol) were dissolved in anhydrous DMF (3 mL) and stirred at rt for 12 h. The mixture was diluted with EtOAc (5 mL) and water (5 mL). The organic layer was dried over Na_2SO_4 and evaporated *in vacuo*. The crude product was purified using preparative HPLC (MeCN/H_2O with 0.1% TFA) yielding 42 mg (64%) of **22**: ^{1}H NMR (400 MHz, DMSO-d_6) δ 12.64 (s, 1H), 7.53 (s, 1H), 7.63–7.21 (m, 6H), 7.02 (d, J = 12.3 Hz, 1H), 6.93 (s, 1H), 4.49 (s, 2H), 3.79–3.69 (m, 6H), 3.32–3.20 (m, 4H), 2.93 (t, J = 6.9 Hz, 2H); ^{13}C NMR (101 MHz, DMSO-d_6) δ 164.37, 161.98, 152.84, 152.74, 138.49, 128.25, 127.51, 127.40, 109.94, 109.05, 105.23, 104.97, 104.64, 104.40, 71.78, 68.59, 65.84, 47.69, 31.60; HRMS (ESI-MS) Calc.: 442.15952 for $C_{23}H_{25}O_3N_3S_1$ [M + H$^+$], Found: 442.15896.

7.1.13. General procedure for the preparation of thiazol-pyrazole-ureas [31,32]

A Schlenk tube was flushed with argon and charged with **8a** (or derivatives), dry DMSO and DIPEA. The reaction mixture was stirred at rt for 10 min before carbamate **15a** was added in one portion. The reaction mixture was heated to 60 °C for overnight. After cooling to rt the mixture was portioned between EtOAc and H_2O. The aqueous layer was then extracted with EtOAc (3 × 10 mL). The combined organic layer was washed with brine and H_2O, dried over Na_2SO_4 and evaporated *in vacuo*. Unless otherwise noted, the crude product was purified using preparative HPLC (MeCN/H_2O with 0.1% TFA).

*7.1.13.1. N-{4-[2-(Benzyloxy)ethyl]-1,3-thiazol-2-yl}-N′-[3-tert-butyl-1-(4-methylphenyl)-1H-pyrazol-5-yl]urea (**16a**).* Prepared as described above in the general procedure using **8a** (40 mg, 0.15 mmol), **15a** (67 mg, 0.15 mmol), DIPEA (80 μL, 0.45 mmol) and DMSO (2 mL). The product was obtained as 14 mg (19%) of an off-white solid: ^{1}H NMR (400 MHz, DMSO-d_6) δ 7.46–7.41 (m, 2H), 7.34–7.21 (m, 7H), 6.81 (bs, 1H), 6.50 (s, 1H), 4.48 (s, 2H), 3.61 (bs, 2H), 2.82 (bs, 2H), 2.38 (s, 3H), 1.31 (s, 9H); ^{13}C NMR (101 MHz, DMSO-d_6) δ 160.67, 158.79, 150.41, 148.17, 138.46, 137.05, 136.27, 135.71, 129.77, 128.20, 127.46, 127.36, 124.48, 107.40, 94.81, 71.71, 68.35, 32.06, 31.43, 30.22, 20.63; HRMS (ESI-MS) Calc.: 490.22712 for $C_{27}H_{32}O_2N_5S$ [M + H$^+$], Found: 490.22695.

*7.1.13.2. N-[3-tert-Butyl-1-(4-methylphenyl)-1H-pyrazol-5-yl]-N′-(4-{2-[(4-fluorobenzyl)oxy]ethyl}-1,3-thiazol-2-yl)urea (**16b**).* Prepared as described above in the general procedure using **8b** (43 mg, 0.15 mmol), **15a** (60 mg, 0.15 mmol), DIPEA (101 μL, 0.59 mmol) and DMSO (2 mL). The crude product was purified using silica gel chromatography (1% MeOH/CH_2Cl_2) yielding 17 mg (22%) of **16b**: ^{1}H NMR

(400 MHz, DMSO-d_6) δ 10.84 (s, 1H), 8.98 (s, 1H), 7.38 (d, J = 8.4 Hz, 2H), 7.31 (m, 4H), 7.13 (t, J = 8.9 Hz, 2H), 6.74 (s, 1H), 6.41 (s, 1H), 4.43 (s, 2H), 3.59 (t, J = 6.4 Hz, 2H), 2.76 (t, J = 6.6 Hz, 2H), 2.36 (s, 3H), 1.27 (s, 9H); ^{13}C NMR (101 MHz, DMSO-d_6) δ 162.68, 160.66, 160.26, 150.36, 148.12, 137.04, 136.25, 135.70, 134.67, 129.76, 129.52 ($^3J_{C-F}$ = 8.2 Hz, 2C), 124.47, 114.95 ($^2J_{C-F}$ = 21.2 Hz, 2C), 107.40, 94.79, 70.90, 68.29, 32.05, 31.37, 30.20, 20.62; HRMS (ESI-MS) Calc.: 508.21770 for $C_{27}H_{31}O_2N_5F_1S_1$ [M + H$^+$], Found: 508.21688.

*7.1.13.3. N-[3-tert-Butyl-1-(4-methylphenyl)-1H-pyrazol-5-yl]-N′-{4-[2-(4-pyridinylmethoxy)ethyl]-1,3-thiazol-2-yl}urea (**16c**).* Prepared as described above in the general procedure using **8c** (40 mg, 0.15 mmol), **15a** (60 mg, 0.15 mmol), DIPEA (101 μL, 0.59 mmol) and DMSO (2 mL). The product was obtained as 12 mg (16%) of an off-white solid: ^{1}H NMR (400 MHz, DMSO-d_6) δ 10.90 (bs, 1H), 9.01 (bs, 1H), 8.50 (d, J = 5.8 Hz, 2H), 7.38 (d, J = 8.4 Hz, 2H), 7.32 (d, J = 8.3 Hz, 2H), 7.26 (d, J = 5.6 Hz, 2H), 6.76 (s, 1H), 6.40 (s, 1H), 4.51 (s, 2H), 3.65 (t, J = 6.5 Hz, 2H), 2.80 (d, J = 6.5 Hz, 2H), 2.36 (s, 3H), 1.27 (s, 9H); ^{13}C NMR (101 MHz, DMSO-d_6) δ 160.66, 157.98, 157.68, 150.55, 149.43, 147.74, 137.03, 136.24, 135.74, 129.76, 124.43, 121.74, 107.51, 95.01, 70.00, 68.87, 32.06, 31.32, 30.21, 20.63; HRMS (ESI-MS) Calc.: 491.22237 for $C_{26}H_{31}O_2N_6S_1$ [M + H$^+$], Found: 491.22154.

*7.1.14. General procedure for the preparation of thiazolo-pyrazole-urea-acids (**16d**–**h**)*

A Schlenk tube was flushed with argon and charged with **8a**, anhydrous DMSO and DIPEA. The reaction mixture was stirred at rt for 10 min before carbamate (**15b**–**f**) was added in one portion. The reaction mixture was heated to 60 °C for overnight. After cooling to rt the mixture was portioned between EtOAc and H_2O. The aqueous layer was extracted with EtOAc (3 × 10 mL). The combined organic layer was washed with brine and H_2O, dried over Na_2SO_4 and evaporated *in vacuo*. The residue was redissolved in MeOH/H_2O (1:1) and an aqueous solution of LiOH (2 eq.) was added. The reaction mixture was stirred for 1–2 h and then diluted with EtOAc and diluted formic acid. The organic layer was dried over Na_2SO_4, before the volatiles were removed *in vacuo*. The crude product was then purified using preparative HPLC (MeCN/H_2O with 0.1% TFA).

*7.1.14.1. [3-(5-{[({4-[2-(Benzyloxy)ethyl]-1,3-thiazol-2-yl}amino) carbonyl]amino}-3-cyclopropyl-1H-pyrazol-1-yl)phenyl]acetic acid (**16d**).* Prepared as described above in the general procedure using **8a** (88 mg, 0.33 mmol), **15b** (150 mg, 0.33 mmol), DIPEA (168 μL, 0.98 mmol), DMSO (2 mL), LiOH (17 mg, 0.66 mmol) and MeOH/H_2O (2 mL). The crude product was purified twice using preparative HPLC (MeCN/H_2O with 0.1% TFA) to furnish 16 mg (9%) of **16d**: ^{1}H NMR (400 MHz, DMSO-d_6) δ 12.31 (bs, 1H), 10.87 (bs, 1H), 8.93 (s, 1H), 7.48–7.23 (m, 9H), 6.74 (s, 1H), 6.19 (s, 1H), 4.45 (s, 2H), 3.67 (s, 2H), 3.62 (t, J = 6.7 Hz, 2H), 2.78 (t, J = 6.6 Hz, 2H), 1.94–1.84 (m, 1H), 0.92–0.85 (m, 2H), 0.73–0.66 (m, 2H); ^{13}C NMR (101 MHz, DMSO-d_6) δ 173.23, 163.75, 159.55, 155.35, 139.31, 138.75, 137.39, 137.34, 129.95, 129.46, 129.05, 128.31, 128.21, 126.40, 123.11, 108.26, 95.80, 72.54, 69.21, 41.09, 32.21, 10.25, 8.61. HRMS (ESI-MS) Calc.: 518.18565 for $C_{27}H_{28}O_4N_5S$ [M + H$^+$], Found: 518.18488.

*7.1.14.2. [4-(5-{[({4-[2-(Benzyloxy)ethyl]-1,3-thiazol-2-yl}amino)carbonyl]amino}-3-tert-butyl-1H-pyrazol-1-yl)phenyl]acetic acid (**16e**).* Prepared as described above in the general procedure using **8a** (44 mg, 0.15 mmol), **15c** (70 mg, 0.15 mmol), DIPEA (75 μL, 0.44 mmol), DMSO (2 mL), LiOH (17 mg, 0.66 mmol) and MeOH/H_2O (2 mL). The crude product was purified using preparative HPLC (MeCN/H_2O with 0.1% TFA) to furnish 23 mg (29%) of the white solid **16e**: ^{1}H NMR (400 MHz, DMSO-d_6) δ 9.01 (s, 1H), 7.45 (d, J = 8.5 Hz, 2H), 7.40 (d, J = 8.6 Hz, 2H), 7.34–7.18 (m, 5H), 6.74 (s, 1H), 6.42 (s, 1H), 4.45 (s, 2H), 3.65 (s, 2H), 3.61 (t, J = 6.7 Hz, 2H), 2.77 (t, J = 6.6 Hz, 2H), 1.28 (s, 9H); ^{13}C NMR (101 MHz, DMSO-d_6) δ 173.29, 161.69, 159.72, 151.51, 148.70, 139.30, 137.60, 137.12, 135.25, 131.17, 129.04, 128.30, 128.20, 125.05, 108.24, 96.01, 72.55, 69.20, 32.91, 32.20, 31.02, 30.44. HRMS (ESI-MS) Calc.: 534.21695 for $C_{28}H_{32}O_4N_5S$ [M + H$^+$], Found: 534.21614.

*7.1.14.3. [3-(5-{[({4-[2-(Benzyloxy)ethyl]-1,3-thiazol-2-yl}amino) carbonyl]amino}-3-cyclopentyl-1H-pyrazol-1-yl)phenyl]acetic acid (**16g**).* Prepared as described above in the general procedure using **8a** (22 mg, 0.09 mmol), **15e** (60 mg, 0.13 mmol), DIPEA (83 μL, 0.49 mmol), DMSO (2 mL), LiOH (8 mg, 0.28 mmol) and MeOH/H_2O (2 mL). The crude product was purified using preparative HPLC (MeCN/H_2O with 0.1% TFA) to furnish 11 mg (22%) of **16g**: ^{1}H NMR (400 MHz, DMSO-d_6) δ 10.90 (bs, 1H), 9.01 (bs, 1H), 8.50 (d, J = 5.8 Hz, 2H), 7.38 (d, J = 8.4 Hz, 2H), 7.32 (d, J = 8.3 Hz, 2H), 7.26 (d, J = 5.6 Hz, 2H), 6.76 (s, 1H), 6.40 (s, 1H), 4.51 (s, 2H), 3.65 (t, J = 6.5 Hz, 2H), 2.80 (d, J = 6.5 Hz, 2H), 2.36 (s, 3H), 1.27 (s, 9H); ^{13}C NMR (101 MHz, DMSO-d_6) δ 160.66, 157.98, 157.68, 150.55, 149.43, 147.74, 137.03, 136.24, 135.74, 129.76, 124.43, 121.74, 107.51, 95.01, 70.00, 68.87, 32.06, 31.32, 30.21, 20.63; HRMS (ESI-MS) Calc.: 491.22237 for $C_{26}H_{31}O_2N_6S_1$ [M + H$^+$], Found: 491.22154.

*7.1.14.4. [3-(5-{[({4-[2-(Benzyloxy)ethyl]-1,3-thiazol-2-yl}amino) carbonyl]amino}-3-tert-butyl-1H-pyrazol-1-yl)phenyl]acetic acid (**16f**).* Prepared as described above in the general procedure using **8a** (32 mg, 0.12 mmol), **15d** (70 mg, 0.15 mmol), DIPEA (33 μL, 0.18 mmol), DMSO (2 mL), LiOH (6 mg, 0.24 mmol) and MeOH/H_2O (2 mL). The crude product was purified using preparative HPLC (MeCN/H_2O with 0.1% TFA) to furnish 23 mg (35%) of **16f**: ^{1}H NMR (400 MHz, DMSO-d_6) δ 9.02 (s, 1H), 7.49–7.23 (m, 9H), 6.75 (s, 1H), 6.43 (s, 1H), 4.46 (s, 2H), 3.68 (s, 2H), 3.62 (t, J = 6.7 Hz, 2H), 2.79 (t, J = 6.7 Hz, 2H), 1.29 (s, 9H); ^{13}C NMR (101 MHz, DMSO-d_6) δ 172.43, 160.94, 158.80, 158.45, 158.10, 138.48, 138.06, 136.49, 136.35, 129.12, 128.64, 128.21, 127.48, 127.37, 125.63, 122.46, 107.41, 95.29, 71.72, 68.39, 40.30, 32.10, 31.40, 30.21; HRMS (ESI-MS) Calc.: 534.21695 for $C_{28}H_{32}O_4N_5S_1$ [M + H$^+$], Found: 534.21622.

*7.1.14.5. [4-(5-{[({4-[2-(Benzyloxy)ethyl]-1,3-thiazol-2-yl}amino) carbonyl]amino}-3-cyclopentyl-1H-pyrazol-1-yl)phenyl]acetic acid (**16h**).* Prepared as described above in the general procedure using **8a** (22 mg, 0.08 mmol), **15f** (60 mg, 0.13 mmol), DIPEA (63 μL, 0.37 mmol), DMSO (2 mL), LiOH (11 mg, 0.5 mmol) and MeOH/H_2O (2 mL). The crude product was purified using preparative HPLC (MeCN/H_2O with 0.1% TFA) to furnish 28 mg (64%) of **16h**: ^{1}H NMR (400 MHz, DMSO-d_6) δ 8.97 (s, 1H), 7.49–7.37 (m, 3H), 7.35–7.23 (m, 6H), 6.74 (s, 1H), 6.37 (s, 1H), 4.45 (s, 2H), 3.67 (s, 2H), 3.61 (t, J = 6.6 Hz, 2H), 3.07–2.98 (t, J = 6.7 Hz, 2H), 2.03–1.93 (m, 2H), 1.76–1.58 (m, 6H); ^{13}C NMR (101 MHz, DMSO-d_6) δ 172.46, 158.60, 156.65, 138.51, 137.99, 136.55, 129.18, 128.68, 128.25, 127.52, 127.42, 125.64, 125.49, 122.38, 107.48, 96.12, 71.76, 68.40, 40.32, 32.73, 31.40, 25.04; HRMS (ESI-MS) Calc.: 546.21695 for $C_{29}H_{32}O_4N_5S_1$ [M + H$^+$], Found: 546.21675.

*7.1.15. 2-{2-[(tert-Butoxycarbonyl)amino]-1,3-thiazol-4-yl}ethyl 4-methylbenzenesulfonate (**9**)*

7 (350 mg, 0.41 mmol) was dissolved in ice-cold anhydrous pyridine (5 mL) and a solution of tosylchloride (78 mg, 0.41 mmol) in anhydrous pyridine (3 mL) was added dropwise. The reaction mixture was stirred at rt for 3h. The mixture was diluted with EtOAc (5 mL) and water (5 mL) and the organic layer was extracted with EtOAc (3 × 5 mL). The organic layer was then dried over Na_2SO_4 and evaporated *in vacuo*. The crude product was purified using column

chromatography (DCM/MeOH 2%) yielding 115 mg (20%) of **9**: ^{1}H NMR (400 MHz, DMSO-d_6) δ 11.28 (s, 1H), 7.65 (d, J = 8.3 Hz, 2H), 7.40 (d, J = 8.3 Hz, 2H), 6.75 (s, 1H), 4.23 (t, J = 6.3 Hz, 2H), 2.85 (t, J = 6.3 Hz, 2H), 2.40 (s, 3H), 1.48 (s, 9H); ^{13}C NMR (101 MHz, DMSO-d_6) δ 159.46, 152.74, 146.07, 144.78, 132.10, 130.03, 127.46, 108.78, 80.98, 69.39, 30.56, 27.91, 21.12; HRMS (ESI-MS) Calc.: 399.10429 for $C_{17}H_{23}O_5N_2S_2$ [M + H$^+$], Found: 399.10405.

7.1.16. *tert-Butyl 4-[2-(3-pyridinylmethoxy)ethyl]-1,3-thiazol-2-ylcarbamate (**10**)*

9 (46 mg, 0.12 mmol), 3-pyridinemethanol (12.6 μL 0.13 mmol) and NaH (10 mg, 0.26 mg) were suspended in anhydrous THF (3 mL) and stirred at rt for 2h. The mixture was diluted with EtOAc (5 mL) and water (5 mL). The organic layer was dried over Na_2SO_4 and evaporated *in vacuo*. The crude product was purified using column chromatography (EtOAc/petroleum ether 60%) yielding 17 mg (43%) of **10**: ^{1}H NMR (400 MHz, DMSO-d_6) δ 11.34 (s, 1H), 8.49 (s, J = 5.8 Hz, 2H), 7.70 (d, J = 7.8 Hz, 1H), 7.37 (dd, J = 7.7, 4.8 Hz, 1H), 6.78 (s, 1H), 4.51 (s, 2H), 3.70 (t, J = 6.8 Hz, 2H), 2.83 (t, J = 6.8 Hz, 2H), 1.46 (s, 9H); ^{13}C NMR (101 MHz, DMSO-d_6) δ 159.12, 152.75, 148.81, 148.69, 148.29, 135.45, 133.90, 123.50, 107.71, 80.91, 69.30, 68.77, 31.51, 27.91; HRMS (ESI-MS) Calc.: 336.13764 for $C_{16}H_{22}O_3N_3S$ [M + H$^+$], Found: 336.13772.

7.1.17. *N-[3-tert-Butyl-1-(4-methylphenyl)-1H-pyrazol-5-yl]-N′-{4-[2-(3-pyridinylmethoxy)ethyl]-1,3-thiazol-2-yl}urea (**16i**)*

10 (17 mg, 0.05 mmol) was dissolved in a 4 M HCl solution in dioxan (2 mL) and stirred for 24h. The amine was then used in the general procedure as described above. 4-(2-(pyridin-3-ylmethoxy) ethyl)thiazol-2-amine (14 mg, 0.05 mmol), **15a** (31 mg, 0.08 mmol), DIPEA (26 μL, 0.15 mmol) and DMSO (2 mL). The crude product was purified using preparative HPLC (MeCN/H_2O with 0.1% TFA) yielding 4 mg (16%) of **16i**: ^{1}H NMR (400 MHz, DMSO-d_6) δ 10.83 (s, 1H), 8.97 (bs, 1H), 8.50–8.47 (m, 2H), 7.68 (d, J = 7.4 Hz, 1H), 7.40–7.30 (m, 5H), 6.75 (s, 1H), 6.40 (s, 1H), 4.50 (s, 2H), 3.63 (t, J = 6.7 Hz, 2H), 2.77 (t, J = 6.7 Hz, 2H), 2.36 (s, 3H), 1.27 (s, 9H); ^{13}C NMR (101 MHz, DMSO-d_6) δ 161.50, 149.61, 149.50, 137.89, 137.09, 136.54, 136.27, 134.71, 130.61, 129.94, 125.33, 124.31, 108.28, 91.24, 70.09, 69.38, 32.90, 31.05, 30.46, 21.47; 2 signals were not seen in the ^{13}C NMR, but were found in HSQC and HMBC spectra: 159.62, 148.96; HRMS (ESI-MS) Calc.: 491.22237 for $C_{26}H_{31}O_2N_6S$ [M + H$^+$], Found: 491.22167.

7.2. Protein expression, purification and labeling

Non-phosphorylated (inactive) human p38α MAP kinase was expressed and purified as described previously [9]. Briefly, an N-terminal His-p38α construct containing the mutations required for specific labeling of the activation loop (C119S/C162S/A172C), as well as wild type p38α, were transformed into BL21(DE3) *E. coli*, over-expressed at 18 °C and purified by Ni-affinity, anion exchange and size exclusion chromatography. The pure protein was subsequently concentrated to ~10 mg/mL and used for fluorescence labeling as described elsewhere [9].

7.3. Endpoint and kinetic measurements

Fluorescent-labeled p38α (50 nM) and various concentrations of inhibitor (1 nM–10 μM) were incubated in the dark at 4 °C for 5h before endpoint fluorescence measurements were carried out in polystyrene cuvettes to determine the K_D of each compound. Long incubation times were required to avoid the K_D time-dependence of type II and III inhibitors binding slowly to p38α [14]. All samples were prepared in FLiK Measurement Buffer (50 mM Hepes, 200 mM NaCl, pH 7.45) and the % v/v DMSO did not exceed 0.2% after addition of inhibitor to cuvettes. All measurements were carried out with a JASCO FP-6500 fluorescence spectrophotometer (JASCO GmbH, Groβ-Umstadt, Germany). For acrylodan-labeled p38α, dual-wavelength ratiometric fluorescence intensity values ($R = I_{\lambda514}/I_{\lambda468}$) enabled reliable binding curves to be plotted against a logarithmic scale of inhibitor concentration to directly determine the K_D of ligand binding. Moreover, binding kinetics were investigated by following the change of emission at 468 nm as described elsewhere [9]. Briefly, the rate constant for association (k_{obs}) was obtained from the decrease of fluorescence after addition of inhibitor, which was fit to a first-order decay function. The addition of 20-fold molar excess of unlabeled p38α to acrylodan-labeled p38α which was pre-incubated with inhibitor led to the dissociation of ligand. The resulting increase in fluorescence was fit to a first-order function and allowed for direct determination of k_{off}.

7.4. IC_{50} determination

p38α was activated according to methods previously reported in literature [33]. 100 μL p38α (14.4 mg/mL) and 41.6 μL active MKK6 (T207E, T211E) (1.4 mg/mL) were diluted to 1.0 mL (total volume) with activation Buffer (50 mM Tris (pH 7.4), 10 mM $MgCl_2$, 1 mM DTT, 0.001% Tween 20) and incubated with 1 mM ATP at 37 °C for 90 min with constant gentle agitation. ATP was subsequently removed by overnight dialysis in buffer containing 25 mM Tris (pH 8.0), 150 mM NaCl, and 10% (v/v) glycerol.

IC_{50} determinations for p38α kinase were measured with the HTRF® KinEASE™-STK assay kit from Cisbio according to the manufacturer's instructions. Active p38α was incubated with inhibitor solution for 2h, before GST-tagged ATF2 substrate and ATP (5 μM) were added. Both, ATP and substrate concentrations were set at the K_M values. For detection, anti-ATF2 and anti-GST-D2 solution was added. A Tecan Safire^2 plate reader was used to measure the fluorescence of the samples at 620 nm (Eu-labeled antibody) and 665 nm (anti-GST-D2) 60 μs after excitation at 317 nm. The ratio of both intensities was calculated in the presence of 8 different inhibitor concentrations (also without inhibitor), was plotted against inhibitor concentrations and fit to a Hill 4-parameter equation to determine IC_{50}-values. At least three independent determinations of each IC_{50} were made, each time in duplicates.

7.5. Protein crystallography

Various inhibitors were co-crystallized with wild type p38α using conditions similar to those described previously [9]. Briefly, protein-inhibitor complexes were prepared by mixing 40 μL p38α (10 mg/mL) with 0.4 μL of inhibitor (100 mM in DMSO) and incubating the mixture for 1h on ice. Samples were centrifuged at 13,000 rpm for 5 min to remove excess inhibitor. In some cases, co-crystallization carried out in the presence of excess inhibitor improved occupancy of the compounds in the crystal structure. Crystals were grown in 24-well crystallization plates using the hanging drop vapor diffusion method and by mixing 1.5 μL protein-inhibitor solution with 0.5 μL reservoir (100 mM MES pH 5.6–6.2, 20–30% PEG4000 and 50 mM *n*-octyl-β-D-glucopyranoside).

7.6. Structure determination, refinement and crystallographic statistics

For the crystals of p38α with inhibitors, 20% glycerol was used as cryo protectant before they were flash frozen in liquid nitrogen. Diffraction data of the p38α-dasatinib, p38α-**18a** and p38α-**16e** complex crystals were measured in-house (Bruker AXS microstar), all other datasets were collected at the PX10SA beamline of the Swiss Light Source (PSI, Villingen, Switzerland) using wavelengths

Table 3
Crystallographic statistics.

	p38α with dasatinib (31fa)	p38α with **13** (31fb)	p38α with **10f** (31fc)	p38α with **10a** (31fd)	p38α with **10c** (31fe)	p38α with **14a** (31ff)	p38α with **10d** (3pg3)
Data collection							
Space group	$P2_1,2_1,2_1$	$P2_12_12_1$	$P2_12_12_1$	$P2_12_12_1$	$P2_12_12_1$	$P2_12_12_1$	$P2_12_12_1$
Cell dimensions							
a, *b*, *c* (Å)	69.06, 69.78, 74.57	67.12, 69.89, 74.43	67.22, 69.09, 74.62	67.95,69.85,74.71	68.63,70.16, 74.18	63.39, 68.75, 74.27	69.11,69.97, 74.53
a, β, γ (°)	90.00, 90.00, 90.00	90.00, 90.00, 90.00	90.00, 90.00, 90.00	90.00, 90.00, 90.00	90.00, 90.00, 90.00	90.00, 90.00, 90.00	90.00, 90.00, 90.00
Resolution (Å)	40.0–2.10 (2.20–2.10)[a]	40.0–2.60 (2.70–2.60)[a]	40.0–2.80 (2.90–2.80)[a]	40.0–3.40 (3.50–3.40)[a]	40.0–2.30 (2.40–2.30)[a]	40.0–1.50 (1.60–1.50)[a]	45.0–2.00 (2.10–2.00)[a]
R_{sym} or R_{merge} (%)	3.5(16.0)	5.3 (31.5)	6.5 (46.0)	15.9 (43.9)	7.0 (36.8)	4.5 (35.1)	6.0 (41.7)
$I/\sigma I$	29.6 (9.4)	23.9 (5.1)	21.5 (3.8)	12.1 (4.7)	15.2 (4.1)	20.3 (4.6)	19.8(4.9)
Completeness (%)	97.6 (95.9)	99.2 (99.7)	95.7 (96.7)	99.2 (99.9)	99.6 (98.2)	99.8 (99.9)	98.7 (98.3)
Redundancy	4.15(4.11)	3.7 (3.7)	3.3 (3.3)	3.9 (3.9)	4.4 (4.2)	5.6 (4.8)	4.4 (4.5)
Refinement							
Resolution (Å)	40.0–2.10	32.8–2.60	34.5–2.80	40.0–3.40	40.0–2.30	40.0–1.50	45.0–2.00
No. reflections	21131	11149	8600	5174	16400	52549	24717
R_{work}/R_{free}	20.2/25.4	23.0/32.0	23.4/32.6	22.2/30.5	21.4/27.4	23.0/24.1	22.0/26.1
No. atoms							
Protein	2674	2682	2690	2662	2687	2678	2714
Ligand/ion	53	45	58	55	55	68	55
Water	148	26	9	-	76	248	99
B-factors	25.4	36.5	39.5	32.1	29.6	18.2	29.6
Protein	25.2	36.7	39.6	32.0	29.5	17.5	29.3
Ligand/ion	31.3	33.4	37.2	35.2	38.8	17.4	28.3
Water	27.2	36.5	27.7	–	29.6	26.1	30.3
R.m.s deviations							
Bond lengths (Å)	0.013	0.009	0.008	0.007	0.013	0.007	0.009
Bond angles (°)	1.456	1.253	1.261	1.185	1.526	1.243	1.176
Wavelength (Å)	1.54170	1.54170	1.54170	1.000000	0.978900	0.978946	1.040000
Temperature	100K	100K	100K	90K	90K	90K	90K
X-ray source	Bruker AXS Microstar	Bruker AXS Microstar	Bruker AXS Microstar	SLS	SLS	SLS	SLS
Ramachandran plot: Residues in							
most favored regions	88.9%	86.3%	87.0%	85.6%	88.7%	91.4%	89.1%
additional allowed regions	10.1%	13.0%	13.0%	14.1%	11.0%	7.9%	9.9%
generously allowed regions	1.0%	0.7%	0.0%	0.3%	0.3%	0.3%	0.7%
disallowed regions	0.0%	0.0%	0.0%	0.0%	0.0%	0.3%	0.3%

[a] Values in paranthesis are for the highest resolution shell.

close to 1 Å. All datasets were processed with XDS and scaled using XSCALE [34]. All p38α-inhibitor complex structures were solved by molecular replacement with PHASER [35] using the published p38α structures (PDB code: 1ZYJ) [36] or (PDB-code: 2EWA) [37] as templates. The molecules in the asymmetric unit were manually modified using the program COOT [38]. The model was first refined with CNS [39] using simulated annealing to reduce model bias. The final refinement was performed with REFMAC5 [40]. Inhibitor topology files where generated using the Dundee PRODRG2 server [41]. Refined structures were validated with PROCHECK [42]. Data collection, structure refinement statistics, PDB-ID codes and further details for the data collection as well as Ramachandran plot results are shown in Table 3. PyMOL [43] was used to produce the figures.

7.7. Cell culture

HeLa cells were cultured in 12-well plates containing Dulbecco's modified Eagle's medium (DMEM) supplemented with 10% heat-inactivated fetal bovine serum (FBS) and 100 units/mL penicillin/streptomycin at 37 °C in humidified air containing 5% CO_2. When the cells reached 80–90% confluence, they were treated with different concentrations of inhibitors or DMSO respectively for 2 h in serum free medium and then stimulated with anisomycin (10 μg/mL final concentration) for 30 min. After removal of the medium, the cells were lysed for 20 min on ice in 50 μL Lysis Buffer (Fermentas, ProteoJET™ Mammalian Cell Lysis Reagent, K0301) containing Roche complete protease inhibitor cocktail tablet according to manufacturer's instruction. The cell lysates were then combined with 15 μL 5X SDS-PAGE loading buffer. The proteins were separated by SDS-PAGE and transferred to nitrocellulose membranes. Blots were blocked and labeled following the manual of MaxTag Kit for Duplex IRDYE Immunoblotting (Rockland, KFA011). For detection of both MK2 and phosphorylated MK2 (pMK2), MK2 antibodies (Cell Signaling, 3042) were used as primary antibodies. For loading control, monoclonal anti-α-tubulin antibody (Sigma, T5168) was used. For confirmation of the pMK2, pMK2 (Thr334) rabbit monoclonal antibody (Cell Signaling, 3007) was used (data not shown). The blots were scanned by using Odyssey Infrared Scanner (Li-COR Biosciences). The images were analyzed using AlphaEaseFC software (Alpha Innotech). The signals of MK2 and pMK2 were together set as 100% (for each sample) and the percentages of MK2 and phosphorylated MK2 were calculated. The data were fit using Origin 7.5 (Origin Lab) with the fit sigmoidal function.

Acknowledgments

J.R.S. was funded by the Alexander von Humboldt Foundation. W.A.L.v.O. thanks the Alexander von Humboldt Foundation for

a Georg Forster Research Fellowship for Experienced Researchers and the University of the Witwatersrand for sabbatical leave. This work was supported by the German Federal Ministry for Education and Research (BMBF 01GS08104). Merck Sharp & Dome, Bayer HealthCare Pharmaceuticals, Merck-Serono and Bayer CropScience are thanked for financial support.

References

[1] E.F. Wagner, A.R. Nebreda, Signal integration by JNK and p38 MAPK pathways in cancer development, Nat. Rev. Cancer 9 (2009) 537–549.
[2] R.J. Mayer, J.F. Callahan, p38 MAP kinase inhibitors: a future therapy for inflammatory diseases, Drug Discov. Today 3 (2006) 49–54.
[3] S. Margutti, S.A. Laufer, Are MAP kinases drug targets? yes, but difficult ones, ChemMedChem 2 (2007) 1116–1140.
[4] J. Zhang, F.J. Adrian, W. Jahnke, S.W. Cowan-Jacob, A.G. Li, R.E. Iacob, T. Sim, J. Powers, C. Dierks, F. Sun, G.R. Guo, Q. Ding, B. Okram, Y. Choi, A. Wojciechowski, X. Deng, G. Liu, G. Fendrich, A. Strauss, N. Vajpai, S. Grzesiek, T. Tuntland, Y. Liu, B. Bursulaya, M. Azam, P.W. Manley, J.R. Engen, G.Q. Daley, M. Warmuth, N.S. Gray, Targeting Bcr-Abl by combining allosteric with ATP-binding-site inhibitors, Nature 463 (2010) 501–506.
[5] Y. Liu, N.S. Gray, Rational design of inhibitors that bind to inactive kinase conformations, Nat. Chem. Biol. 2 (2006) 358–364.
[6] R.A. Copeland, D.L. Pompliano, T.D. Meek, Drug-target residence time and its implications for lead optimization, Nat. Rev. 5 (2006) 730–739.
[7] S. Klüter, C. Grütter, T. Naqvi, M. Rabiller, J.R. Simard, V. Pawar, M. Getlik, D. Rauh, Displacement assay for the detection of stabilizers of inactive kinase conformations, J. Med. Chem. 53 (2010) 357–367.
[8] J.R. Simard, S. Klüter, C. Grütter, M. Getlik, M. Rabiller, H.B. Rode, D. Rauh, A new screening assay for allosteric inhibitors of cSrc, Nat. Chem. Biol. 5 (2009) 394–396.
[9] J.R. Simard, M. Getlik, C. Grütter, V. Pawar, S. Wulfert, M. Rabiller, D. Rauh, Development of a fluorescent-tagged kinase assay system for the detection and characterization of allosteric kinase inhibitors, J. Am. Chem. Soc. 131 (2009) 13286–13296.
[10] J.R. Simard, M. Getlik, C. Grütter, R. Schneider, S. Wulfert, D. Rauh, Fluorophore labeling of the glycine-rich loop as a method of identifying inhibitors that bind to active and inactive kinase conformations, J. Am. Chem. Soc. 132 (2010) 4152–4160.
[11] J.R. Simard, C. Grütter, V. Pawar, B. Aust, A. Wolf, M. Rabiller, S. Wulfert, A. Robubi, S. Klüter, C. Ottmann, D. Rauh, High-throughput screening to identify inhibitors which stabilize inactive kinase conformations in p38alpha, J. Am. Chem. Soc. 131 (2009) 18478–18488.
[12] J. Rudolph, L.D. Cantin, S. Magnuson, W. Bullock, A.M. Bullion, L. Chen, C.Y. Chuang, S. Liang, D. Majumdar, H. Ogutu, A. Olague, N. Qi, P.L. Wickens, Anilinopyrazole Derivatives Useful for the Treatment of Diabetes, WO 2004/050651, 2004.
[13] M. Getlik, C. Grütter, J.R. Simard, S. Klüter, M. Rabiller, H.B. Rode, A. Robubi, D. Rauh, Hybrid compound design to overcome the gatekeeper T338M mutation in cSrc, J. Med. Chem. 52 (2009) 3915–3926.
[14] C. Pargellis, L. Tong, L. Churchill, P.F. Cirillo, T. Gilmore, A.G. Graham, P.M. Grob, E.R. Hickey, N. Moss, S. Pav, J. Regan, Inhibition of p38 MAP kinase by utilizing a novel allosteric binding site, Nat. Struct. Biol. 9 (2002) 268–272.
[15] M. Goedert, A. Cuenda, M. Craxton, R. Jakes, P. Cohen, Activation of the novel stress-activated protein kinase SAPK4 by cytokines and cellular stresses is mediated by SKK3 (MKK6); comparison of its substrate specificity with that of other SAP kinases, EMBO J. 16 (1997) 3563–3571.
[16] R. Ben-Levy, S. Hooper, R. Wilson, H.F. Paterson, C.J. Marshall, Nuclear export of the stress-activated protein kinase p38 mediated by its substrate MAPKAP kinase-2, Curr. Biol. 8 (1998) 1049–1057.
[17] E. ter Haar, P. Prabhakar, X. Liu, C. Lepre, Crystal structure of the p38 alpha-MAPKAP kinase 2 heterodimer, J. Biol. Chem. 282 (2007) 9733–9739.
[18] J.F. Schindler, J.B. Monahan, W.G. Smith, p38 pathway kinases as anti-inflammatory drug targets, J. Dent. Res. 86 (2007) 800–811.
[19] Y. Shi, M. Gaestel, In the cellular garden of forking paths: how p38 MAPKs signal for downstream assistance, Biol. Chem. 383 (2002) 1519–1536.
[20] M.W. Karaman, S. Herrgard, D.K. Treiber, P. Gallant, C.E. Atteridge, B.T. Campbell, K.W. Chan, P. Ciceri, M.I. Davis, P.T. Edeen, R. Faraoni, M. Floyd, J.P. Hunt, D.J. Lockhart, Z.V. Milanov, M.J. Morrison, G. Pallares, H.K. Patel, S. Pritchard, L.M. Wodicka, P.P. Zarrinkar, A quantitative analysis of kinase inhibitor selectivity, Nat. Biotechnol. 26 (2008) 127–132.
[21] J.S. Tokarski, J.A. Newitt, C.Y. Chang, J.D. Cheng, M. Wittekind, S.E. Kiefer, K. Kish, F.Y. Lee, R. Borzillerri, L.J. Lombardo, D. Xie, Y. Zhang, H.E. Klei, The structure of dasatinib (BMS-354825) bound to activated ABL kinase domain elucidates its inhibitory activity against imatinib-resistant ABL mutants, Cancer Res. 66 (2006) 5790–5797.
[22] M. Kaspadya, V.K. Narayanaswamyb, M. Raju, G.K. Rao, Synthesis, antibacterial activity of 2,4-disubstituted oxazoles and thiazoles as bioisosteres, Lett. Drug Des Discov. 6 (2009) 21–28.
[23] C.E. Fitzgerald, S.B. Patel, J.W. Becker, P.M. Cameron, D. Zaller, V.B. Pikounis, S.J. O'Keefe, G. Scapin, Structural basis for p38alpha MAP kinase quinazolinone and pyridol-pyrimidine inhibitor specificity, Nat. Struct. Biol. 10 (2003) 764–769.
[24] M. Rabiller, M. Getlik, S. Klüter, A. Richters, S. Tückmantel, J.R. Simard, D. Rauh, Proteus in the world of proteins: conformational changes in protein kinases, Arch. Pharm. (Weinheim) 343 (2010) 193–206.
[25] A.C. Backes, B. Zech, B. Felber, B. Klebl, G. Müller, Small-molecule inhibitors binding to protein kinases. Part I: exceptions from the traditional pharmacophore approach of type I inhibition, Expert Opin. Drug Discovery 3 (2008) 1409–1425.
[26] A.C. Backes, B. Zech, B. Felber, B. Klebl, G. Müller, Small-molecule inhibitors binding to protein kinase. Part II: the novel pharmacophore approach of type II and type III inhibition, Expert Opin. Drug Discovery 3 (2008) 1427–1449.
[27] J. Regan, S. Breitfelder, P. Cirillo, T. Gilmore, A.G. Graham, E. Hickey, B. Klaus, J. Madwed, M. Moriak, N. Moss, C. Pargellis, S. Pav, A. Proto, A. Swinamer, L. Tong, C. Torcellini, Pyrazole urea-based inhibitors of p38 MAP kinase: from lead compound to clinical candidate, J. Med. Chem. 45 (2002) 2994–3008.
[28] H.O. Kim, M. Kahn, The synthesis of aminoazole analogs of lysine and arginine: the Mitsunobu reaction with lysinol and argininol, Synlett (1999) 1239–1240.
[29] D.E. Ryono, P.T.W. Cheng, S.A. Bolton, S. Chen, Y. Shi, W. Meng, J.A. Tino, H. Zhang, R.B. Sulsky, Novel Glucokinase Activators and Methods of Using Same, US2008/9465, 2008.
[30] A.L. Gill, M.G. Carr, J.F. Lyons, N.T. Thompson, D.C. Rees, 5-Morpholinymethylthiophenyl Pharmaceutical Compounds as p38 MAP Kinase Modulators, WO2005/100338, 2005.
[31] M.C. Bagley, T. Davis, M.C. Dix, C.S. Widdowson, D. Kipling, Microwave-assisted synthesis of *N*-pyrazole ureas and the p38alpha inhibitor BIRB 796 for study into accelerated cell ageing, Org. Biomol. Chem. 4 (2006) 4158–4164.
[32] L.H. Zhang, L. Zhu, Novel Process for Synthesis of Heteroaryl-substituted Urea Compounds, WO/2001/004115, 2001.
[33] J.E. Sullivan, G.A. Holdgate, D. Campbell, D. Timms, S. Gerhardt, J. Breed, A.L. Breeze, A. Bermingham, R.A. Pauptit, R.A. Norman, K.J. Embrey, J. Read, W.S. VanScyoc, W.H. Ward, Prevention of MKK6-dependent activation by binding to p38alpha MAP kinase, Biochemistry 44 (2005) 16475–16490.
[34] W. Kabsch, Automatic processing of rotation diffraction data from crystals of initially unknown symmetry and cell constants, J. Appl. Cryst. 26 (1993) 795–800.
[35] R.J. Read, Pushing the boundaries of molecular replacement with maximum likelihood, Acta Crystallogr. D Biol. Crystallogr. 57 (2001) 1373–1382.
[36] E.L. Michelotti, K.K. Moffett, D. Nguyen, M.J. Kelly, R. Shetty, X. Chai, K. Northrop, V. Namboodiri, B. Campbell, G.A. Flynn, T. Fujimoto, F.P. Hollinger, M. Bukhtiyarova, E.B. Springman, M. Karpusas, Two classes of p38alpha MAP kinase inhibitors having a common diphenylether core but exhibiting divergent binding modes, Bioorg. Med. Chem. Lett. 15 (2005) 5274–5279.
[37] M. Vogtherr, K. Saxena, S. Hoelder, S. Grimme, M. Betz, U. Schieborr, B. Pescatore, M. Robin, L. Delarbre, T. Langer, K.U. Wendt, H. Schwalbe, NMR characterization of kinase p38 dynamics in free and ligand-bound forms, Angew. Chem. Int. Ed. Engl. 45 (2006) 993–997.
[38] P. Emsley, K. Cowtan, Coot: model-building tools for molecular graphics, Acta Crystallogr. D Biol. Crystallogr. 60 (2004) 2126–2132.
[39] A.T. Brünger, P.D. Adams, G.M. Clore, W.L. DeLano, P. Gros, R.W. Grosse-Kunstleve, J.S. Jiang, J. Kuszewski, M. Nilges, N.S. Pannu, R.J. Read, L.M. Rice, T. Simonson, G.L. Warren, Crystallography & NMR system: a new software suite for macromolecular structure determination, Acta Crystallogr. D Biol. Crystallogr. 54 (1998) 905–921.
[40] G.N. Murshudov, A.A. Vagin, E.J. Dodson, Refinement of macromolecular structures by the maximum-likelihood method, Acta Crystallogr. D Biol. Crystallogr. 53 (1997) 240–255.
[41] A.W. Schuttelkopf, D.M. van Aalten, PRODRG: a tool for high-throughput crystallography of protein-ligand complexes, Acta Crystallogr. D Biol. Crystallogr. 60 (2004) 1355–1363.
[42] R.A. Laskowski, M.W. McArthur, D.S. Moss, J.M. Thornton, PROCHECK: a program to check the stereochemical quality of protein structures, J. Appl. Crystallogr. 26 (1993) 263–291.
[43] W.L. DeLano, The PyMOL Molecular Graphics System (2002). http://www.pymol.org.